

ALMA MATER STUDIORUM · UNIVERSITÀ DI BOLOGNA

Dipartimento di Fisica e Astronomia
Corso di Laurea in Fisica

Characterization of a superconducting qubit in a resonant cavity for the Qub-IT experiment

Relatore:
Dott. Matteo Franchini

Presentata da:
Carlo Mattia Lovecchio

Anno Accademico 2023/2024

Contents

Abstract	4
Introduction	6
1 QUBIT THEORY	7
1.1 Qubits	7
1.2 Multiple qubits	8
1.2.1 Quantum noise	9
1.3 Quantum computation	10
1.3.1 Single quantum gates	10
1.3.2 Multiple quantum gates	12
2 THE TRANSMON QUBIT	15
2.1 One-dimensional cavity modes	15
2.2 Transmon qubit	18
2.3 Qubit-cavity interaction	23
2.4 Qubit dynamics and Qubit driving	28
3 QUB-IT PROJECT	32
3.1 INFN's Superconducting Qubit	32
3.2 Qubit characterization	38
3.2.1 Input Output Theory	39
3.2.2 One-Tone Spectroscopy	44
3.2.3 Two-Tone Spectroscopy	46
3.2.4 Rabi Measurements	48
3.2.5 T1 Measurements	55
Conclusions	60

Abstract

Negli ultimi anni i computer quantistici hanno compiuto grandi progressi, con sempre nuove applicazioni in vari settori. Al centro del calcolo quantistico vi è il qubit, o quantum bit. Il progetto Qub-IT dell'INFN mira a sviluppare sensori quantistici basati su qubit superconduttori per la rilevazione della materia oscura, sfruttando misurazioni Quantum Non-Demolition (QND). Questa tesi si concentra sulla caratterizzazione di un qubit superconduttore del tipo Xmon, integrato in una cavità risonante. Il qubit è stato caratterizzato nel Frascati National Laboratory (FNL) dove nel maggio 2024 sono state effettuate le misure di caratterizzazione del qubit, ovvero la spettroscopia One-Tone e Two-Tone, oscillazioni di Rabi e misurazioni del tempo di rilassamento T1. Ho analizzato i dati raccolti per valutare le prestazioni del qubit. I risultati di questa tesi contribuiscono alla comprensione delle potenzialità del qubit nell'ambito del quantum sensing, con implicazioni per futuri esperimenti di fisica fondamentale.

*Alla nonna Vita,
A Michela, Alle Chiare,
E a tutti quelli che mi hanno sostenuto*

Introduction

In recent years, quantum computing has emerged as one of the most promising technologies. In past years we have seen enormous progress in this field, with new application of quantum computers in many fields, from cryptography to artificial intelligence or physics simulations. Central to this technology is the qubit, quantum equivalent of the bit in classical computing, it's the fundamental element of the quantum computer. Between the many implementations of the qubit, the superconducting qubits, known for their coherence and scalability, are leading the charge in this revolution.

In 2022 the INFN (National Institute of Nuclear Physics in Italy) started the Qub-IT project, aimed to develop quantum sensing with superconducting qubits for present and future INFN fundamental-physics experiments. The main objective of the project is the realization of an itinerant single-photon counter that surpasses present devices in terms of efficiency and low dark-count rates by exploiting repeated Quantum non-demolition (QND) measurements of a single photon and entanglement in multiple qubits. The device will find immediate application in light dark-matter searches. The project sees the participation of several universities, INFN units and research institutes. Specifically this project consists in the design and construction of a Xmon qubit, a type of superconducting Transmon qubit consisting of a Josephson Junction integrated with a resonant cavity.

Between the 6th and the 15th of May, the qubit has been characterized with various experiments. This thesis aims to analyze the data of the qubit characterization of the superconducting qubit within the Qub-it experiment, with the goal of understanding its performance and potential for future applications in quantum sensing.

In the first chapter I will talk about the theoretical overview of the qubit, their properties, how they differ from the classical qubit and how to manipulate them.

In the second chapter I will provide a detailed explanation of the transmon qubit, the resonant cavity and their interaction.

In the third chapter I will talk about the Xmon qubit of the Qub-it project, about the qubit characterization and the theory of the data analysis. I analyzed the data taken in May using the numpy library of Python, as the data were saved in a ".npz" format. The qubit characterization includes experiments such as One-Tone spectroscopy, Two-tone spectroscopy, Rabi oscillations and T_1 measurements.

Chapter 1

QUBIT THEORY

1.1 Qubits

A qubit, or quantum bit, is an essential element of quantum computation and quantum information. Just like its classical counterpart, the bit, it can be in the state $|0\rangle$ or in the state $|1\rangle$, called computational basis states. The main difference between the two is that the bit has only two possible states, 0 or 1, while the qubit has a continuum of states, each of which is formed by a different linear combination of the states $|0\rangle$ and $|1\rangle$. These are represented by the Dirac notation and are called superpositions:

$$|\psi\rangle = \alpha |0\rangle + \beta |1\rangle \quad (1.1)$$

where α and β are complex numbers. The state of a qubit can be represented as a two-dimensional vector. So the qubit is able to exist in a superposition of states, it can be in both state $|0\rangle$ and $|1\rangle$ simultaneously, until it is measured. The act of measuring the qubit causes the qubit to collapse in one of the two states. When the qubit is measured, it will result $|0\rangle$ with probability $|\alpha|^2$ and $|1\rangle$ with probability $|\beta|^2$. As the probabilities must sum to 1, it is required that $|\alpha|^2 + |\beta|^2 = 1$. It is not possible to determine the quantum state $|\psi\rangle$ of a qubit through measurement. The act of the measurement gives us a definite outcome, $|0\rangle$ or $|1\rangle$, but gives us no information about α or β . We need multiple identical copies of $|\psi\rangle$ and perform various measurement to determine an approximation of the two values. This process is called quantum state tomography.

The states $|0\rangle$ and $|1\rangle$ can be represented by various physical systems. For example, the spin of an electron can be $+1/2$ or $-1/2$, where $+1/2$ corresponds to $|1\rangle$ and $-1/2$ to $|0\rangle$. The same can be said for the polarization of photons, the two states of an electron orbiting an atom [1].

An example of a qubit state is the one called $|+\rangle$, where the qubit has equal probabilities of being 0 or 1 when measured:

$$|+\rangle = \frac{1}{\sqrt{2}} |0\rangle + \frac{1}{\sqrt{2}} |1\rangle \quad (1.2)$$

One useful geometric representation is the Bloch sphere. Because $|\alpha|^2 + |\beta|^2 = 1$, it is possible to write the qubit state as:

$$|\psi\rangle = e^{i\gamma} \left(\cos \frac{\theta}{2} |0\rangle + e^{i\varphi} \sin \frac{\theta}{2} |1\rangle \right) \quad (1.3)$$

In Eq.1.3, the factor $e^{i\gamma}$ can be ignored since it has no observable effects. So it is possible to write:

$$|\psi\rangle = \cos \frac{\theta}{2} |0\rangle + e^{i\varphi} \sin \frac{\theta}{2} |1\rangle \quad (1.4)$$

The real numbers θ and φ define a point on the surface of a unit three-dimensional sphere, called the Bloch sphere. θ represent the zenith angle and φ is the azimuthal angle. These represent the position of the qubit on the sphere, where the poles correspond to $|0\rangle$ (north pole) and $|1\rangle$ (south pole).

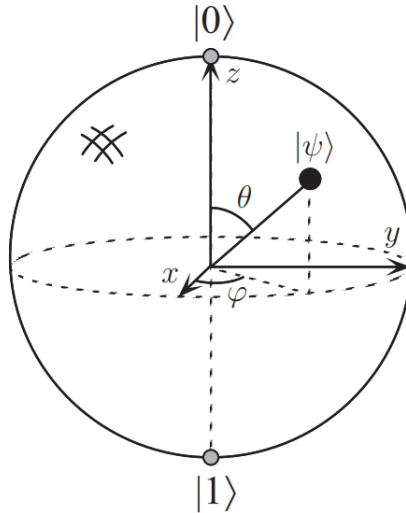


Figure 1.1: Bloch sphere representation of a qubit. On the north pole is placed the $|0\rangle$ state, while in the south is the $|1\rangle$ state. The angles represent the state of the qubit.

1.2 Multiple qubits

In quantum computation it is essential to work with multiple qubits. The computational basis states of two qubits are $|00\rangle, |01\rangle, |10\rangle, |11\rangle$ that represent every possible combi-

nation of the states of the single qubits. The state of the system is a linear combination of the basis states:

$$|\psi\rangle = \alpha_{00}|00\rangle + \alpha_{01}|01\rangle + \alpha_{10}|10\rangle + \alpha_{11}|11\rangle \quad (1.5)$$

where the constants are normalized, since we are in a quantum system. So we have the condition $\sum_x |\alpha_x|^2 = 1$, where $|\alpha_x|^2$ represent the probability of finding the state in the $|x\rangle$ state.

After measuring one of the two qubit the system changes, as we remove some combinations. For example, if we measure the first qubit and it results in $|0\rangle$, the only combinations possible for the system are $|00\rangle$ and $|01\rangle$. So the state can be represented as the linear combination of these two states, renormalized as to have the total probability equal to one.

$$|\psi\rangle = \frac{\alpha_{00}|00\rangle + \alpha_{01}|01\rangle}{\sqrt{|\alpha_{00}|^2 + |\alpha_{01}|^2}} \quad (1.6)$$

This state is called a post-measurement state.

An example of an important two-qubit state is the Bell state:

$$|\psi\rangle = \frac{|00\rangle + |11\rangle}{\sqrt{2}} \quad (1.7)$$

The Bell state has half probability of being in the state $|00\rangle$ and half of being in the state $|11\rangle$.

This state has an amazing property, when one of the qubits is measured, the state of the other qubit is instantly determined. It is important to understand that in quantum mechanics, when we refer to superposition, we mean that the system can be in multiple states with different probabilities. It is not that we are unaware of the state of the system, but rather it has no definite state, until it is measured. Its state is determined only when it is measured. The property that we are referring to in the Bell state is that when one qubit is measured, we know also the measurement of the other qubit. This occurs simultaneously, independently of the distance between the two qubits. This phenomenon is called entanglement, and the two qubits are said to be entangled.

This property is the reason why the Bell state is so used in quantum computation, as it is the main feature that allows quantum "teleportation".

1.2.1 Quantum noise

In quantum computing the number of possible measured states corresponds to qubit combinations that grow exponentially with the number of qubits. For n qubit there are 2^n combinations, so the state becomes a vector of 2^n components, with basis of the form $|x_1, x_2, \dots, x_n\rangle$. The largest quantum computer ever built has just a few hundreds qubits.

So, for example, if a system has $n=600$, that means that it has 2^{600} possible states, an enormous amount of information, and more than a classical computer could ever dream of computing and efficiently simulate.

A great amount of qubits is necessary to build an efficient quantum computer. This is important to reduce the quantum noise, or quantum decoherence, i.e. the loss of quantum information as qubits interact with their external environment. When this happens, the qubit state can collapse before the reading process, resulting in incorrect calculation or data loss. To resolve this problem it is necessary some strategies of quantum error correction, that requires a significant number of qubits. These extra qubits help detecting errors and correcting them.

Current quantum computers are still in the early stages of error corrections and can only handle a limited amount of qubits with noise. To compute complex tasks it is necessary to build much larger computers with many more qubits. As of 2024, Atom Computing has built the largest quantum computer by qubit count, with their 1,225-qubit machine [8].

1.3 Quantum computation

In quantum computation the logic gates are different from classical logic gates. They are called quantum gates, while the circuitry is represented through quantum circuits.

1.3.1 Single quantum gates

To compute quantum gates it is possible to use vector notation. The state of a single qubit:

$$|\psi\rangle = \alpha |0\rangle + \beta |1\rangle$$

can be written as:

$$\begin{bmatrix} \alpha \\ \beta \end{bmatrix}$$

The quantum gates can be written as matrices. For a single qubit they are 2x2 unitary matrices U , and it follows that:

$$U \begin{bmatrix} \alpha \\ \beta \end{bmatrix} = \begin{bmatrix} \alpha' \\ \beta' \end{bmatrix}$$

The vector obtained is also a quantum state. That means that it must be normalized, so $|\alpha'|^2 + |\beta'|^2 = 1$. This happens only if the matrix is unitary, that is if $U^\dagger U = I$ where U^\dagger is the adjoint of U and I is the identity matrix. This is the only constraint on quantum gates.

An example of quantum gate is the NOT gate, also called X gate, defined as:

$$X = \begin{bmatrix} 0 & 1 \\ 1 & 0 \end{bmatrix}$$

that inverts the states $|0\rangle$ and $|1\rangle$, so after it is applied, we get the state:

$$|\psi\rangle = \alpha |1\rangle + \beta |0\rangle$$

or, in vector notation:

$$X \begin{bmatrix} \alpha \\ \beta \end{bmatrix} = \begin{bmatrix} \beta \\ \alpha \end{bmatrix}$$

The following gates are the most commonly used.
The Z gate:

$$Z = \begin{bmatrix} 1 & 0 \\ 0 & -1 \end{bmatrix}$$

which leaves $|0\rangle$ unchanged and invert the sign of $|1\rangle$:

$$Z \begin{bmatrix} \alpha \\ \beta \end{bmatrix} = \begin{bmatrix} \alpha \\ -\beta \end{bmatrix}$$

The Hadamard gate:

$$H = \frac{1}{\sqrt{2}} \begin{bmatrix} 1 & 1 \\ 1 & -1 \end{bmatrix}$$

which is described as a square root of NOT:

$$H \begin{bmatrix} \alpha \\ \beta \end{bmatrix} = \frac{1}{\sqrt{2}} \begin{bmatrix} \alpha + \beta \\ \alpha - \beta \end{bmatrix}$$

The Hadamard gate is essential in the creation of Bell states.

Every single quantum gate can be represented as a rotation on the Bloch sphere. For example the X gate is a rotation around the X axis and the Z gate is a rotation around the Z axis. In Fig.1.2 it is possible to see the rotation on the block sphere representing the Hadamard gate.

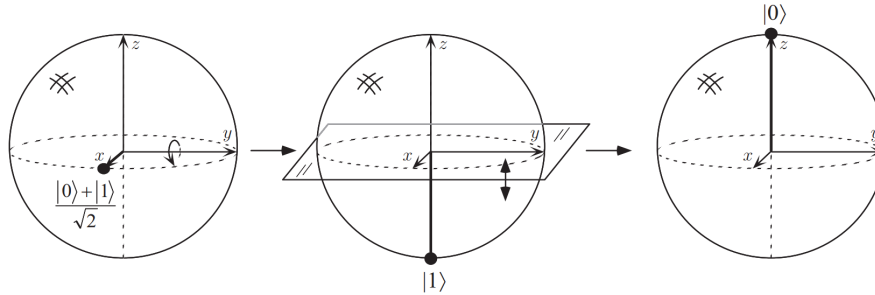


Figure 1.2: A representation of the Hadamard gate on the Bloch Sphere

1.3.2 Multiple quantum gates

In quantum computation, one of the most important multiple qubit gate is the controlled-NOT or CNOT gate. It has two inputs, known as the "target qubit" and "controlled qubit", and two outputs. Practically it is a NOT gate, that invert the state of the target qubit, but with a control. If the control qubit is $|0\rangle$, the NOT is "off" and the target is left as it is. If the control qubit is $|1\rangle$, the target qubit is inverted. The matrix representation of the CNOT gate is:

$$U_{CN} = \begin{bmatrix} 1 & 0 & 0 & 0 \\ 0 & 1 & 0 & 0 \\ 0 & 0 & 0 & 1 \\ 0 & 0 & 1 & 0 \end{bmatrix}$$

It is useful to represent multiple qubits gate using quantum circuit representation, for example the CNOT gate can be seen as:

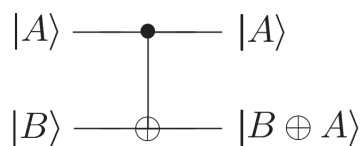


Figure 1.3: Representation of the CNOT quantum circuit

The circuit has to be read from left to right. We start with some qubits and for every qubit there must be a wire connected to it. The wire can represent the passage of time and the evolution of the qubit.

An important example of quantum circuit is the one that creates Bell states. We consider a two qubit system and we apply the Hadamard gate on the first one. Then we

apply a CNOT gate, using the first qubit as the control qubit and the second qubit as the target.

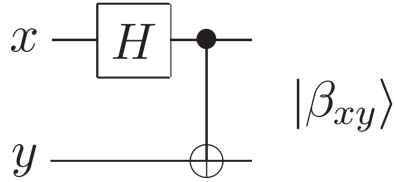


Figure 1.4: Quantum circuit representation of the process to create Bell states

For example, we start with both qubits in the $|0\rangle$ state, so that the total state can be represented by $|00\rangle$. Then we apply the Hadamard gate on the first qubit, this will result in the first qubit changing its state from $|0\rangle$ to a mixed quantum state:

$$|0\rangle \rightarrow \frac{1}{\sqrt{2}}(|0\rangle + |1\rangle) = |+\rangle \quad (1.8)$$

Now the total state can be written as:

$$|00\rangle \rightarrow \frac{1}{\sqrt{2}}(|00\rangle + |10\rangle) \quad (1.9)$$

Then, when the CNOT is applied, we have that:

$$|00\rangle \rightarrow |00\rangle, \quad |10\rangle \rightarrow |11\rangle$$

The system's final state will be:

$$\frac{1}{\sqrt{2}}(|00\rangle + |11\rangle) \quad (1.10)$$

that is a Bell state.

There are other Bell states, one for each combination of the starting qubits. If we start with the qubits in the state $|00\rangle$, we obtain the Bell state:

$$|\beta_{00}\rangle = \frac{1}{\sqrt{2}}(|00\rangle + |11\rangle) \quad (1.11)$$

To $|01\rangle$ corresponds:

$$|\beta_{01}\rangle = \frac{1}{\sqrt{2}}(|01\rangle + |10\rangle) \quad (1.12)$$

To $|10\rangle$ corresponds:

$$|\beta_{10}\rangle = \frac{1}{\sqrt{2}}(|00\rangle - |11\rangle) \quad (1.13)$$

And at last as $|11\rangle$ we get the Bell state:

$$|\beta_{11}\rangle = \frac{1}{\sqrt{2}}(|01\rangle - |10\rangle) \quad (1.14)$$

Chapter 2

THE TRANSMON QUBIT

The qubit produced by the Qub-IT collaboration is called a Transmon qubit, whose fundamental element is the Josephson Junction. This junction interacts with a photon contained in a cavity. The photon must be in a single mode of light, this is achieved by building a cavity that supports a discrete set of modes.

2.1 One-dimensional cavity modes

Using Maxwell's equations it is possible to describe the electromagnetic fields inside the cavity, taking as an example a one-dimensional cavity. Consider a pair of infinite perfect conducting walls separated by the distance L along the z -direction.

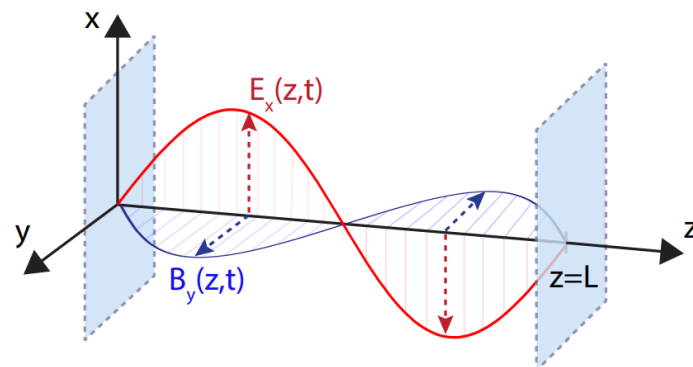


Figure 2.1: A schematic diagram of a one-dimensional cavity.

This configuration can be considered as one-dimensional because we have a continuous translational invariance in x and y dimensions. The electric and magnetic field depend only on the z coordinate. We also assume that the electric field is polarized along x -axis, so the magnetic field must be polarized along the y -axis [3]. In Fig. 2.1 we can see

a representation of the one-dimension cavity. Being an empty cavity, with no external current, it is possible to consider Maxwell's equations as written:

$$\frac{\partial E_x(z, t)}{\partial z} = -\frac{\partial B_y(z, t)}{\partial t} \quad (2.1)$$

$$-\frac{\partial B_y(z, t)}{\partial z} = \mu_0 \epsilon_0 \frac{\partial E_x(z, t)}{\partial t} \quad (2.2)$$

$$\frac{\partial E_x(z, t)}{\partial x} = 0 \quad (2.3)$$

$$\frac{\partial B_y(z, t)}{\partial y} = 0 \quad (2.4)$$

The boundaries conditions are $E_x(z = 0, t) = 0$ and $E_x(L, t) = 0$, for perfect conducting walls, where the electric field has to vanish. So we can find the solution for the electromagnetic field inside the cavity:

$$E_x(z, t) = \mathcal{E} q(t) \sin(kz) \quad (2.5)$$

$$B_y(z, t) = \mathcal{E} \frac{\mu_0 \epsilon_0}{k} \dot{q}(t) \cos(kz) \quad (2.6)$$

where $q(t)$ is the canonical position, and describes the time evolution for modes. \mathcal{E} is the normalization constant, set as $\mathcal{E} = \sqrt{\frac{2\omega_c^2}{V\epsilon_0}}$ where V is the volume of the cavity.

The parameter k is a wave number defined as $k = m\pi/L$, where m is a positive integer. This wave number k correspond to the frequency $\omega_c = \frac{k}{\sqrt{\mu_0 \epsilon_0}}$, where each value of m corresponds to a different mode.

The total energy in the cavity can be described as:

$$H = \frac{1}{V} \int \left(\frac{\epsilon_0}{2} |E_x(z, t)|^2 + \frac{1}{2\mu_0} |B_y(z, t)|^2 \right) dV \quad (2.7)$$

Substituting in the equation for H we get the total energy in function of $p(t)$ and $q(t)$, respectively canonical momentum and position, where $\dot{q}(t) = p(t)$.

$$H = \frac{1}{2} [p^2(t) + \omega_c^2 q^2(t)] \quad (2.8)$$

The normalization constant \mathcal{E} is defined so that the total energy in the cavity find a simple and compact form.

Using the correspondence principle it is possible to treat these classical quantities as quantistic operators. We can find the quantistic Hamiltonian as:

$$\hat{H} = \frac{1}{2} [\hat{p}^2(t) + \omega_c^2 \hat{q}^2(t)] \quad (2.9)$$

In terms of the annihilation and creation operators, the Hamiltonian takes the form:

$$\hat{H} = \omega_c(\hat{a}^\dagger\hat{a} + \frac{1}{2}) = \omega_c(\hat{n} + \frac{1}{2}). \quad (2.10)$$

where we define $\hat{n} = \hat{a}^\dagger\hat{a}$ as the number operator. In the end we obtain:

$$\hat{H} |n\rangle = E_n |n\rangle \quad \text{with} \quad n = 0, 1, 2, \dots$$

where $|n\rangle$ are the photon number states or Fock states and are the energy eigenstate for a single mode cavity field with $E_n = \omega_c(n + \frac{1}{2})$. n represent the number of photons contained inside the cavity. At every moment in time the cavity can be in a state $|n\rangle$ or in a superposition $\sum c_n |n\rangle$. The Fock states is a complete orthogonal basis of the cavity system. So the light inside the cavity can be represented by a wave function $|\psi\rangle$ using Fock states:

$$|\psi\rangle = |n\rangle \quad (2.11)$$

where $n = 0$ means that there is no photon in the cavity. Even in the state $|0\rangle$ has some electromagnetic fluctuation, while the average is zero.

Another useful bases to describe the cavity system is the coherent state basis. It refers to coherent light, that is light waves with the same phase, so the peaks align. This is also called classical light because this is the most common type of light. Coherent light can be represented using the Fock bases:

$$|\psi\rangle = |\alpha\rangle = \sum_n c_n |n\rangle \quad , \quad c_n = e^{-\frac{|\alpha|^2}{2}} \frac{\alpha^n}{\sqrt{n!}} \quad (2.12)$$

where α indicates the average expected number of photons of the coherent state:

$$\langle \hat{n} \rangle = |\alpha|^2 \quad (2.13)$$

The coherent state is the eigenstate of the annihilation operator:

$$\hat{a} |\alpha\rangle = \alpha |\alpha\rangle \quad (2.14)$$

This eigenstates do not form an orthogonal bases.

The coherent state is important because it allows for quantum measurement. The time evolution of this wave function is a rotation around the origin in the phase space, by the frequency of the light ω_c . This represents the oscillation between the magnetic and electric field. It is possible to change the phase space to a rotating frame where the coherent phase is static. In this frame any change or external influence is easily detected as a displacement.

2.2 Transmon qubit

The Transmon qubit is a circuit made up of a capacitor and a Josephson junction (JJ) that introduces an element of non linearity, essential to create a qubit.

The Josephson junction is made of a thin layer of an insulator ($\sim 1\text{nm}$) sandwiched between two superconducting slabs.

In superconductors the current carriers are a pair of electrons with opposite momenta and spins, called Cooper pairs. At low temperature they are found at the lowest energy E_0 and they evolve following the Schrodinger equation in the stationary state. Cooper pair are much larger than the average distance between electrons, so the wave functions of many Cooper pairs overlap. These wave functions that overlap create a macroscopic wave function that can be described by a single complex number:

$$\Psi = \sqrt{n}e^{i\theta} \quad (2.15)$$

where n is the density of the pairs and θ is the common phase [5]. Each superconductor of the Josephson junction has its own density, n_1 and n_2 , and common phase, θ_1 and θ_2 .

Since the insulator barrier is thin enough, there is a non negligible probability that a Cooper pair tunnels through it. This creates a super-current I that exists even at $V = 0$. The JJ can be thought of as a dissipationless non-linear inductor. The I-V characteristics of the JJ are:

$$I = I_0 \sin(\delta) \quad (2.16)$$

$$V = \frac{\Phi_0}{2\pi} \dot{\delta} \quad (2.17)$$

where $\delta = \theta_2 - \theta_1$ and I_0 is the critical current above which the JJ loses the non-linearity of its inductance and becomes a normal dissipative junction. $\Phi_0 = \frac{h}{2e}$ is the magnetic flux quantum. In Fig. 2.2 is depicted the I-V characteristic of the JJ, where it's evident the non-linearity of the junction at low tension and it's possible to see how the current is non-zero at $V = 0$.

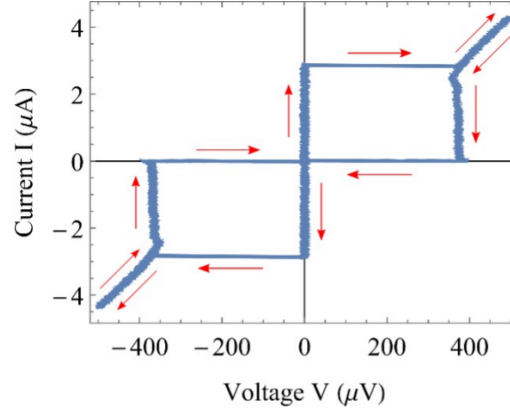


Figure 2.2: I-V characteristic of a Josephson junction

It is possible to find the inductance of the Josephson junction as:

$$V = L \frac{di}{dt} \rightarrow \frac{\Phi_0}{2\pi} \dot{\delta} = LI_0 \dot{\delta} \cos(\delta) \rightarrow L = \frac{\Phi_0}{2\pi I_0 \cos(\delta)} \rightarrow L = \frac{L_{J0}}{\cos(\delta)} \quad (2.18)$$

where L_{J0} is defined as the Josephson inductance at zero current.

It is possible to have a tunable critical current by linking two JJs in a superconducting loop forming a structure called SQUID (Superconducting Quantum Interference Device), represented in Fig.2.3. By passing an external flux Φ_{ext} through the loop, we get:

$$I_0^{SQUID} = 2I_0 \left| \cos\left(\frac{\pi \Phi_{ext}}{\Phi_0}\right) \right| \quad (2.19)$$

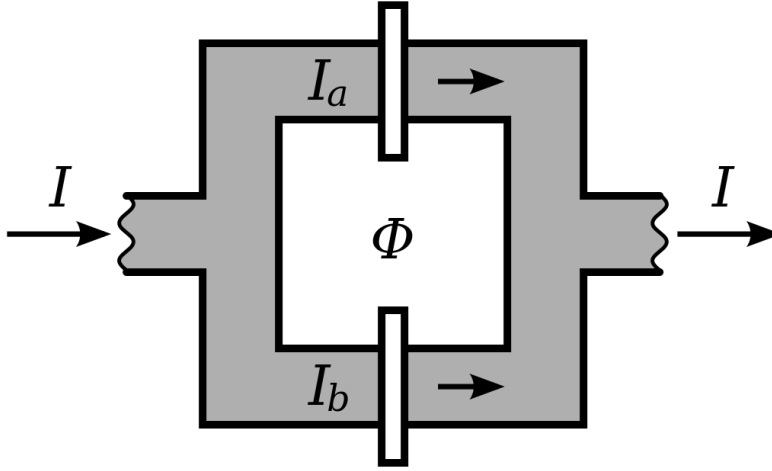


Figure 2.3: SQUID made connecting two JJ in loop

The total energy stored in a JJ is given by integrating the energy changes $\frac{dU}{dt} = VI$:

$$U = \int_{-\infty}^t I(t')V dt' = \frac{I_0\Phi_0}{2\pi} \int_0^{\delta(t)} \sin(\delta)d\delta = E_J[1 - \cos(\delta)] \quad (2.20)$$

where $E_J = \Phi_0 I_0 / 2\pi = \hbar I_0 / 2e$ is the Josephson energy.

By shunting a JJ with a relatively large capacitor, it is possible to create an anharmonic oscillator, that is the Transmon qubit (Fig.2.4) The capacitor has to be large enough so that $E_J \gg E_C$, where $E_C = \frac{e^2}{2C}$.

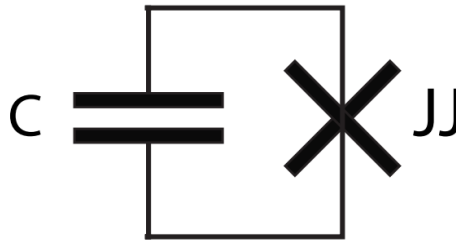


Figure 2.4: Diagram of the Transmon circuit

The difference between an harmonic and anharmonic oscillator is the fact that in an harmonic oscillator the energy difference between consecutive energy levels is constant, while in an anharmonic oscillator this gap increase at each level. This property is essential

to create a qubit because by tuning the difference between the energy levels, this ensures that only the two lowest states are accessible, while the higher states require too much energy to be easily reached.

The total energy of a Transmon circuit is given by:

$$H_{trans} = H_C + H_J = \frac{Q^2}{2C} + E_J[1 - \cos(\delta)] \quad (2.21)$$

where Q is the total charge in the capacitor. It is possible to express the total charge using Cooper pairs as $Q = 2em$, where m is the number of pairs. The total energy can be written in the form:

$$H_{trans} = 4E_C m^2 + E_J[1 - \cos(\delta)] \quad (2.22)$$

the first term can be seen as the kinetic energy stored in the capacitor and the second one the potential energy stored in the JJ. Here m is the canonical momentum and δ the canonical position. Using the correspondence principle we can translate this equation to quantum mechanics:

$$\hat{H}_{trans} = 4E_C \hat{m}^2 + E_J[1 - \cos(\hat{\delta})] \quad (2.23)$$

where this is the Hamiltonian for the transmon qubit system. The next step is to find the eigenvectors and eigenvalues. In the limit where $\delta \ll 1$, the cosine can be expanded up to the 4th order of δ , obtaining the Hamiltonian of an harmonic oscillator plus a nonlinear term, that can be considered a perturbation.

$$\hat{H}_{trans} \approx 4E_C \hat{m}^2 + E_J \frac{\delta^2}{2} - E_J \frac{\delta^4}{24} \quad (2.24)$$

We can consider first only the harmonic oscillator, and add later the perturbation to find the anharmonic oscillation.

$$\hat{H}_{armonic} = 4E_C \hat{m}^2 + E_J \frac{\delta^2}{2} \quad (2.25)$$

the frequency of the harmonic oscillator is $\omega_J = \sqrt{8E_J E_C} / \hbar$.

It is possible to rewrite the energy equation using creation and annihilation operators. We get:

$$\hat{\delta} = \sqrt{\frac{Z_R}{2}}(\hat{b} + \hat{b}^\dagger), \quad \hat{m} = i\sqrt{\frac{1}{2Z_R}}(\hat{b} - \hat{b}^\dagger), \quad Z_R = \sqrt{\frac{8E_C}{E_J}}$$

It is known that the harmonic oscillator Hamiltonian, in annihilation and creation operators, is $\hat{H} = \hbar\omega(\hat{b}^\dagger\hat{b} + \frac{1}{2})$, so we get

$$\hat{H}_{trans} = \hbar\omega_J(\hat{b}^\dagger\hat{b} + \frac{1}{2}) - E_J \frac{\left[\sqrt{\frac{\hbar Z_R}{2}}(\hat{b} + \hat{b}^\dagger)\right]^4}{24} = \hbar\omega_J(\hat{b}^\dagger\hat{b} + \frac{1}{2}) - E_J \frac{\hbar^2 \frac{8E_C}{E_J} (\hat{b} + \hat{b}^\dagger)^4}{24 \cdot 4}$$

$$\hat{H}_{trans} = \hbar\omega_J(\hat{b}^\dagger\hat{b} + \frac{1}{2}) - \frac{\hbar^2 E_C(\hat{b} + \hat{b}^\dagger)^4}{12} \quad (2.26)$$

From the time independent perturbation theory we get:

$$E_n = E_n^0 + V_{nn} \quad (2.27)$$

and to get the perturbation at first order:

$$|n\rangle_1 = |n\rangle + \sum_{k \neq n} \frac{V_{nk}}{E_n^0 - E_k^0} |k\rangle \quad (2.28)$$

where $V_{nk} = \langle n|V|k\rangle$. So we get:

$$E_n = \hbar\omega_J(n + \frac{1}{2}) - \frac{E_C}{12} \langle n|(\hat{b} + \hat{b}^\dagger)^4|n\rangle \quad (2.29)$$

$$|n\rangle_1 = |n\rangle - \frac{E_C}{12} \sum_{k \neq n} \frac{\langle k|(\hat{b} + \hat{b}^\dagger)^4|n\rangle}{\hbar\omega_J(n - k)} \quad (2.30)$$

We can compute V_{nn} to find the energy levels:

$$\langle n|(\hat{b} + \hat{b}^\dagger)^4|n\rangle = \langle n|(6\hat{b}^\dagger\hat{b}\hat{b}^\dagger\hat{b} + 6\hat{b}^\dagger\hat{b} + 3)|n\rangle \quad (2.31)$$

so that we get:

$$E_n = \hbar\omega_J(n + \frac{1}{2}) - \frac{E_C}{12}(6n^2 + 6n + 3) \quad (2.32)$$

The energy difference between two consecutive levels is

$$E_{n,n+1} = \hbar\omega_{n,n+1} = E_{n+1} - E_n = \hbar\omega_J - (n + 1)E_C \quad (2.33)$$

The anharmonicity α is:

$$\alpha = E_{12} - E_{01} = -E_C \quad (2.34)$$

and the transmon frequency is:

$$\hbar\omega_T = \hbar\omega_J - E_C = \sqrt{8E_J E_C} - E_C \quad (2.35)$$

By choosing a reasonable anharmonicity $\alpha = E_{12} - E_{01} \sim -300MHz$, we can consider only the first two level, 0 and 1.

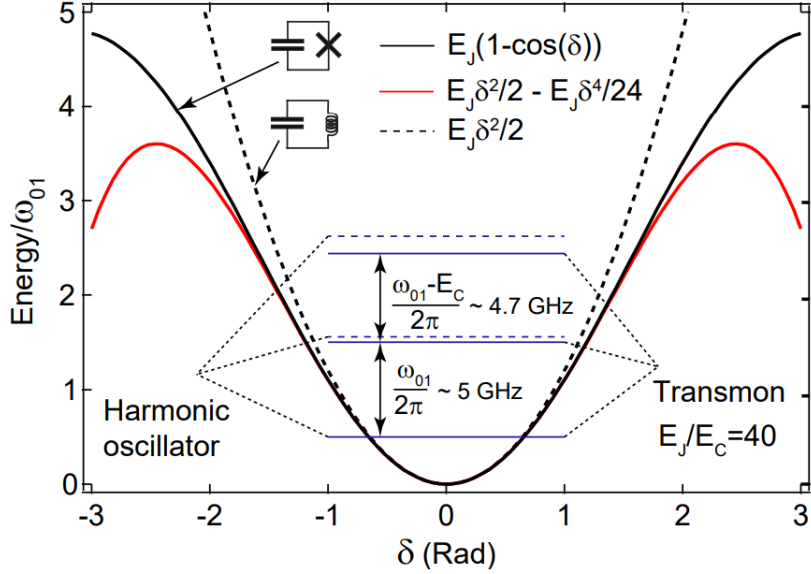


Figure 2.5: A transmon potential in comparison with a non linear oscillator and an harmonic oscillator

2.3 Qubit-cavity interaction

To study the qubit-cavity system, we need to find the total Hamiltonian:

$$\hat{H} = \hat{H}_{cavity} + \hat{H}_{qubit} + \hat{H}_{int} \quad (2.36)$$

where H_{int} is the Hamiltonian of the interaction between the cavity and the qubit. Since we tune the qubit so that it can be found only in two possible states, its Hamiltonian can be described using Pauli operator:

$$\hat{H}_{qubit} = -\frac{\omega_q}{2} \hat{\sigma}_z \quad (2.37)$$

where ω_q is the lowest frequency transition in the transmon qubit.

To define the Hamiltonian of the interaction, we consider the cavity at the lowest mode. So we consider the cavity with a single photon ($n=1$), where the cavity has the minimum frequency and the maximum electromagnetic amplitude at the center of the cavity. We put the qubit in the middle of the cavity, at $z = L/2$, where L is the length of the cavity. Since the qubit is so small, we can consider the interaction only with the electromagnetic field at $z = L/2$. The qubit interacts via its electric dipole moment to the electric field of the cavity. The Hamiltonian of the interaction is defined as:

$$\hat{H}_{int} = -\hat{d} \cdot \hat{E}_x(L/2, t) \quad (2.38)$$

where $\hat{d} = \begin{pmatrix} 0 & d \\ d^* & 0 \end{pmatrix}$, and d is a parameter indicating the magnitude of the electric dipole of the qubit and d^* is its conjugate. Considering the dipole aligned at the x axis with the electric field of the cavity, we can define d_x as the magnitude of dipole. The matrix can be rewritten as $\hat{d} = d_x \sigma_x = d_x (\sigma_+ + \sigma_-)$ where σ_+ is the raising operator of the qubit and σ_- is the lowering operator. We also assume that d_x is a real number.

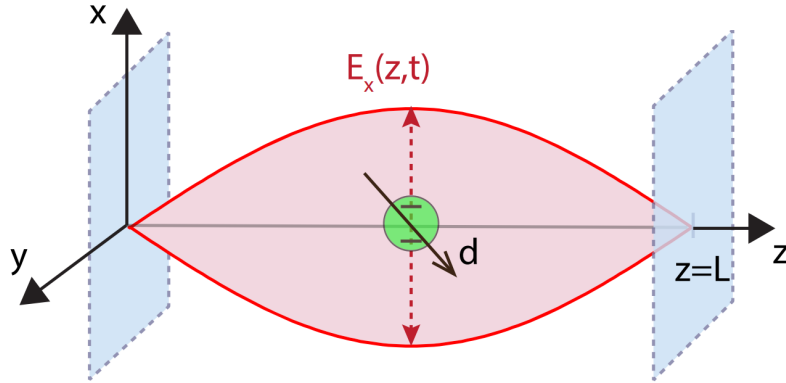


Figure 2.6: Visual representation of the qubit inside the cavity, at $z = L/2$

So, substituting in Eq. 2.36, the total Hamiltonian is:

$$\hat{H} = \omega_c (\hat{a}^\dagger \hat{a} + \frac{1}{2}) - \frac{\omega_q}{2} \hat{\sigma}_z - g (\hat{a} + \hat{a}^\dagger) (\sigma_+ + \sigma_-) \quad (2.39)$$

where we considered the Hamiltonian of the cavity from Eq. 2.10, while $g = d_x E_0$ represent the magnitude of the interaction.

So the qubit can be in two eigenstates: $|g\rangle$, ground state with eigenvalue $-\omega_q/2$, and $|e\rangle$, excited state with eigenvalue $+\omega_q/2$. The cavity has infinite eigenstates $|n\rangle$, corresponding to the number of photons, with eigenvalues $\omega_c(n + 1/2)$.

Let's first consider the case where we have no interaction, so $g = 0$. In this case the state of the system is represented by the tensor product of the qubit and cavity eigenstates, $|g\rangle |n\rangle$ and $|e\rangle |n\rangle$ with eigenvalue $\pm\omega_q/2 + \omega_c(n + 1/2)$. These are called bare states.

In the case of $g \neq 0$, we simplify the Hamiltonian using the rotating wave approximation (RWA), valid when $g \ll \omega_q$, $g \ll \omega_c$ and $|\omega_c - \omega_q| \ll |\omega_c + \omega_q|$. The Hamiltonian of the interaction can be written as:

$$H_{int} = g([\hat{a}^\dagger \sigma_- + \hat{a} \sigma_+] + [\hat{a}^\dagger \sigma_+ + \hat{a} \sigma_-]) \quad (2.40)$$

The first term represents the decay of the qubit while simultaneously generating a photon in the cavity, and the second term describes the excitation of the qubit, accompanied by the absorption of a photon within the cavity. Both the processes conserve the

total energy of the state since the energy change is of a factor $\pm(\omega_c - \omega_q)$, while the total energy is of a factor $(\omega_c + \omega_q)$, so the second is much larger than the first one because of the initial assumption.

The third term represent the excitation of the qubit and the generation of a photon, while the fourth term is the decay of the qubit and the absorption of a photon in the cavity. These two last terms change the energy of the system by a term $(\omega_c + \omega_q)$. Since the energy change is so big compered to the first two interactions, it is much less likely to occur. Following the time-energy uncertainty principle, the bigger the energy exchange is, less the time in which this change happens. So the occurrence of these two last processes are negligible in respect to the first two.

So we can write the Jaynes-Cummings Hamiltonian, that represent the system with interaction in the rotating wave approximation:

$$H_{JC} = \omega_c(\hat{a}^\dagger \hat{a} + \frac{1}{2}) - \frac{\omega_q}{2}\sigma_z - g(\hat{a}^\dagger \sigma_- + \hat{a} \sigma_+) \quad (2.41)$$

We want to find the eigenvectors and eigenvalues of this Hamiltonian. Since the eigenvalues of the cavity goes from 0 to infinity, we have an infinite matrix that we want to diagonalize. This Hamiltonian can be diagonalized in blocks, each eigenvalue of each block will be an eigenvalue of the Hamiltonian. The block of excitation number n is:

$$M_n = \begin{pmatrix} \omega_c(n + 1/2) - \omega_q/2 & g\sqrt{n+1} \\ g\sqrt{n+1} & \omega_c(n + 1/2) + \omega_q/2 \end{pmatrix}$$

Diagonalizing this block matrices we get the so called dressed states.

In the case of $|g\rangle |0\rangle$, so the lowest energy case called the ground state, we get:

$$|0, -\rangle = |g\rangle |0\rangle \quad (2.42)$$

$$E_g = -\frac{\Delta}{2} \quad (2.43)$$

where $\Delta = \omega_q - \omega_c$ is called detuning. For the other cases, where $n=1,2,3,\dots$, we get the eigenstates:

$$|n, -\rangle = \cos\theta_n |g\rangle |n+1\rangle - \sin\theta_n |e\rangle |n\rangle \quad (2.44)$$

$$|n, +\rangle = \sin\theta_n |g\rangle |n+1\rangle + \cos\theta_n |e\rangle |n\rangle \quad (2.45)$$

with eigenvalues

$$E_{\pm} = \omega_c(n + \frac{1}{2}) \pm \frac{1}{2}\sqrt{4g^2(n+1) + \Delta^2} \quad (2.46)$$

where

$$\theta_n = \frac{1}{2}\tan^{-1}\left(\frac{2g\sqrt{n+1}}{\Delta}\right) \quad (2.47)$$

is called level of hybridation. Fig. 2.7 show the behaviour of theta in function of Δ .

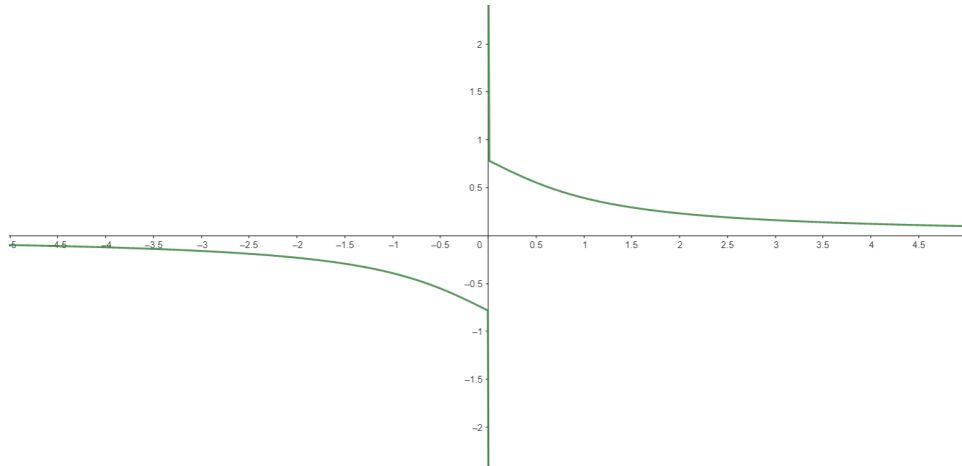


Figure 2.7: Graph representing the curve of the function $y = \frac{1}{2}\tan^{-1}(1/x)$ to show the behaviour of θ_n . At $x \rightarrow 0$ the function reach its maximum, as $x \rightarrow \pm\infty$ the function approaches zero.

By changing Δ we observe all the possible states of the system. This states are represented in Fig. 2.8.

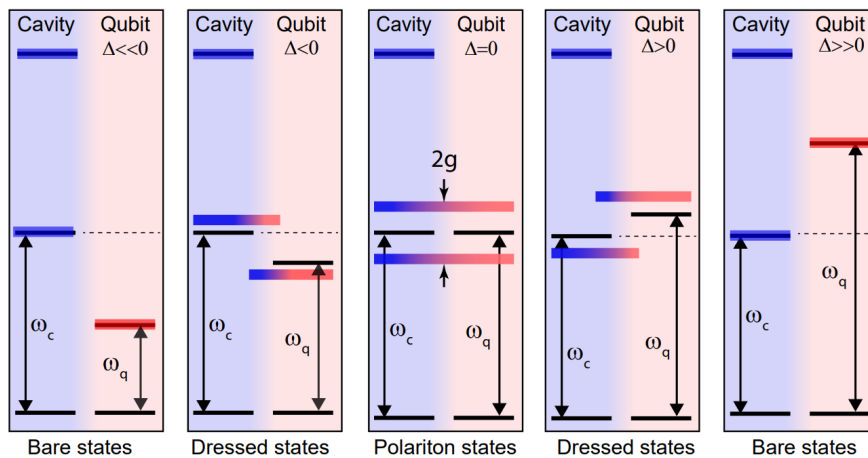


Figure 2.8: In this graph are represented all the possible states of the system. The line in black represent the frequency of the qubit (on the right) and of the cavity (on the left). The colored lines indicate the energy levels of the system. When the frequencies are at the same level we are in the polariton states, where the energy is at the furthest point from the corresponding bare states. As the difference of the frequencies increase, the interaction has less influence on the system.

If $\Delta \sim 0$, we get that $\theta_n = \frac{\pi}{4}$. With this level of hybridation the states are in maximum hybridation:

$$|n, \pm\rangle = \frac{1}{\sqrt{2}} |g\rangle |n+1\rangle \pm \frac{1}{\sqrt{2}} |e\rangle |n\rangle \quad (2.48)$$

these states are called polaritons. The system has half probability of being in the ground state and half of being in the excited state. The polaritons have the lowest energy difference of $2g$.

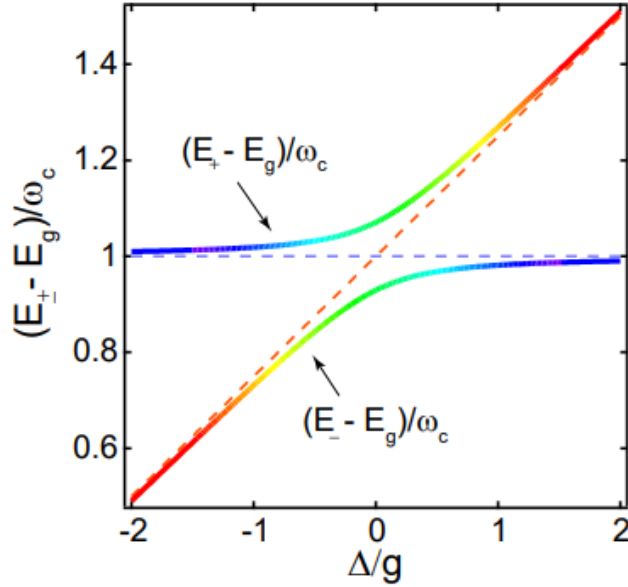


Figure 2.9: Plot of the eigenvalues of the system in function of the detuning. The dashed lines represent the bare states' energy

At $|\Delta| > 0$ the dressed states still have some energy difference from its bare states. At $|\Delta| \gg 0$, we have that $\theta_n \approx 0$. So the dressed states energy is the same of the bare state. It is as if there is no interaction between the cavity and the qubit.

Fig. 2.9 shows the behaviour of the energy of the system in function of Δ and its difference from the bare states.

We conclude that by controlling one of the frequencies, ω_c or ω_q , we can control the state of the system. Typically in a transmon qubit we control ω_q and leave ω_c constant.

Furthermore using the dispersive approximation, available when $\Delta \ll g$, it's possible to find the dispersive Hamiltonian, that is the Hamiltonian for a far detuned qubit-cavity system where the interaction is weak and the dressed state almost overlap with the bare states. This Hamiltonian can be written as:

$$\hat{H}_{dis} = (\omega_c - \chi\sigma_z)\hat{a}^\dagger\hat{a} - \frac{1}{2}\omega_q\sigma_z \quad (2.49)$$

where $\chi = g^2/\Delta$ is called dispersive shift. The dispersive interaction causes a frequency shift of the cavity resonance frequency. When the qubit is in the ground state $|g\rangle$ ($\langle\sigma_z\rangle = 1$) the cavity frequency shifts by $-\chi$, while if the qubit is in the excited state $|e\rangle$ ($\langle\sigma_z\rangle = -1$) the cavity frequency shifts by $+\chi$. This property is very important. since it allows to see if there is an interaction between the qubit and the cavity and it will be used to perform some of the measurements in the qubit characterization.

2.4 Qubit dynamics and Qubit driving

We now want to study the time evolution of the qubit. To do that we are going to ignore the energy of the cavity and focus only on the terms given by the interaction.

We consider the Hamiltonian as:

$$H = H_{qubit} + H_{int} = -\frac{\omega_q}{2}\sigma_z - E(t) \cdot \hat{d} \quad (2.50)$$

Assuming the dipole is aligned with the electric field and that $E(t) = \cos(\omega_d t)E_0$. So we can simplify the equation:

$$H = H_{qubit} + H_{int} = -\frac{\omega_q}{2}\sigma_z - A\cos(\omega_d t)\sigma_x \quad (2.51)$$

where $A = E_0 d_x$ indicates the strength of the interaction. This is a time dependent Hamiltonian. To find how the state evolve in time we must solve the time dependent Schrodinger equation.

This Hamiltonian can be solved using an ansatz. We know that the state must be of the type $|\psi\rangle = C_g |g\rangle + C_e |e\rangle$. The time evolution of this state is given by:

$$|\psi(t)\rangle = C_g(t)e^{i\frac{\omega_q}{2}t} |g\rangle + C_e(t)e^{-i\frac{\omega_q}{2}t} |e\rangle \quad (2.52)$$

Substituting this state in the Schrodinger equation we can find C_g and C_e :

$$i\frac{\partial |\psi(t)\rangle}{\partial t} = \left(-\frac{\omega_q}{2}\sigma_z - A\cos(\omega_d t)\sigma_x \right) |\psi(t)\rangle \quad (2.53)$$

We can find two differential equations:

$$\dot{C}_g = iA\cos(\omega_d t)e^{-i\omega_q t}C_e \quad (2.54)$$

$$\dot{C}_e = iA\cos(\omega_d t)e^{i\omega_q t}C_g \quad (2.55)$$

Since it is possible to write the cosine as a sum of imaginary exponential, we can write:

$$\dot{C}_g = iA(e^{-i(\omega_q - \omega_d)t} + e^{-i(\omega_q + \omega_d)t})C_e$$

$$\dot{C}_e = iA(e^{i(\omega_q - \omega_d)t} + e^{i(\omega_q + \omega_d)t})C_g$$

Using the rotating wave approximation we can simplify these differential equations. As $|\omega_c - \omega_q| \ll |\omega_c + \omega_q|$, $e^{-i(\omega_q - \omega_d)t}$ represent a rotation much slower in frequency than $e^{-i(\omega_q + \omega_d)t}$. We neglect the biggest frequency since we are not interested in short timescales in the dynamics. So we ignore the fast-rotating term and focus on the slowest one, that dominate the behaviour of the system:

$$\dot{C}_g = iAe^{-i(\omega_q - \omega_d)t}C_e \quad (2.56)$$

$$\dot{C}_e = iAe^{i(\omega_q - \omega_d)t}C_g \quad (2.57)$$

Now we can solve analytically and we get the solution:

$$C_g(t) = \frac{e^{-i\frac{\Delta_d}{2}t}}{\Omega_R} \left[\Omega_R \cos\left(\frac{\Omega_R}{2}t\right) + i\Delta_d \sin\left(\frac{\Omega_R}{2}t\right) \right] \quad (2.58)$$

$$C_e(t) = i\frac{Ae^{+i\frac{\Delta_d}{2}t}}{\Omega_R} \sin\left(\frac{\Omega_R}{2}t\right) \quad (2.59)$$

where $\Delta_d = \omega_q - \omega_d$ and $\Omega_R = \sqrt{A^2 + \Delta_d^2}$

We can also find the probability of getting the excited state:

$$P_e(t) = |C_e(t)|^2 = \frac{A^2}{\Omega_R^2} \sin^2\left(\frac{\Omega_R}{2}t\right) \quad (2.60)$$

From this we can conclude that the qubit doesn't respond to a far detuned drive, but as the detuning $\Delta_d \rightarrow 0$, the excitation oscillations grow. This is shown in Fig. 2.10, where it's represented a Chevron plot. A Chevron plot shows the oscillations of the qubit state, in function of time and different frequencies. We can see how the oscillations are more evident at the center of the plot, corresponding to the qubit frequency where Δ_d is near zero. As the frequency changes, we get a bigger Δ_d and lower oscillations. There is also a Chevron plot in function of power, where at higher energy the oscillations are more frequent, and at lower power the oscillation have lower frequency.

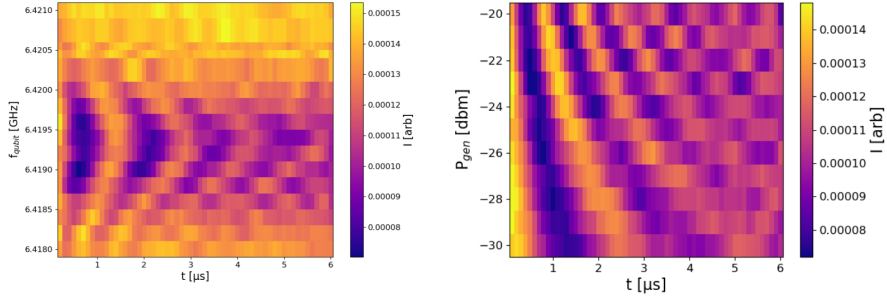


Figure 2.10: On the left a chevron plot in function of the frequency, on the right in function of the power. The color represent the excitement of the qubit in time.

In the ideal case, the qubit remains isolated and continues to oscillate indefinitely. In the real case, since it interact with the external environment, the system dissipate its energy and it stops after some time. This dissipation is caused by two key phenomena: *relaxation* and *dephasing*. Both can be represented on the Bloch Sphere, as seen in Fig. 2.11.

Relaxation is what happens when the qubit interact with the environment and decay to the ground state, losing some of its energy. Preparing the qubit in the excited state, after some time it will find some decay channel and lose a photon. This happens in a random amount of time. As time passes, the chances of the qubit having relaxed a photon increases. This phenomenon can be represented by an exponential distribution. The population of excited states at time t is given by $P_e(t) = P_e(0)e^{-\frac{t}{T_1}}$. T_1 is called relaxation time. It is an important parameter in the qubit characterization and represent the time scale of the decay of the qubit. At $t = T_1$ the population of excited states will have reduced itself by $1/e$.

The dephasing is due to noise sources in the system, that changes randomly the phase of the qubit. It doesn't cause the qubit to relax but it changes the qubit resonance frequency, the qubit rotates around the Z axis on the Bloch sphere. We consider the equation of the qubit state on the Bloch sphere, Eq. 1.4. If in an ideal qubit the phase time evolution is given by $\varphi = \omega_q t$, with decoherence we need to add a random term that represent uncertainty and grows with time:

$$\varphi = \omega_q t + \zeta(t) \quad (2.61)$$

We call T_2^* the dephasing time, the time scale in which the qubit loses its phase coherence. It is characterized by a Ramsey measurement.

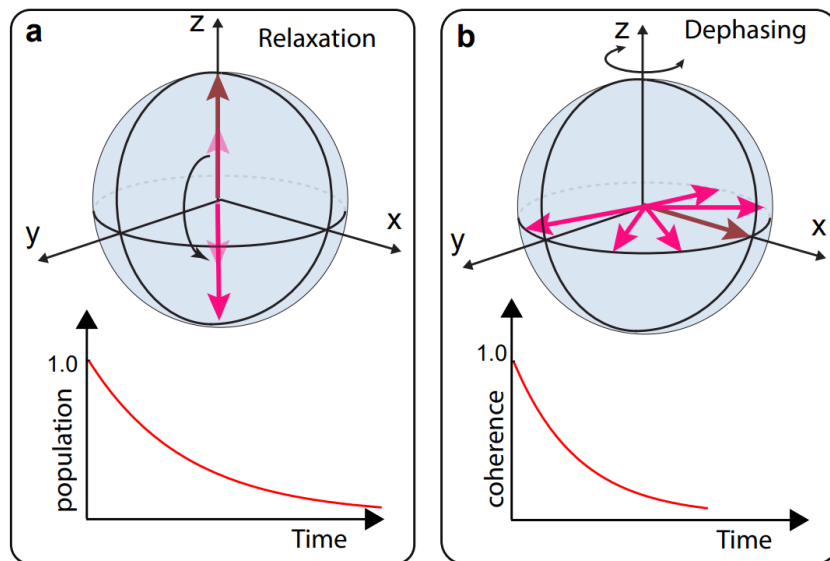


Figure 2.11: Bloch representation of the relaxation and dephasing of the qubit

Chapter 3

QUB-IT PROJECT

In 2022, the INFN (Italian Institute of Nuclear Physics) started the Qub-IT project. The goal of this project is the construction of a microwave single-photon detector using Quantum Non-Demolition measurement (QND), so detecting itinerant single-photons without absorbing it. This type of detector is suitable for the detection of the axion, an hypothetical elementary particle theorized as one of the possible components of Dark Matter. Axions are particles with really low mass and so are difficult to detect. Quantum Sensing with superconducting qubits is a possible way of doing that. It has been shown that superconducting qubits can detect single photons with a few GHz of frequency via the QND. This technique reduces the dark count rate and improve sensitivity in high precision experiments.[10]

3.1 INFN's Superconducting Qubit

The design of the qubit was made using the Qiskit-Metal package, developed by IBM, an open-source framework for the design of superconducting quantum chips. The design of the Qub-IT qubit, made using Qiskit-Metal. can be seen in Fig. 3.1. The qubit built in a laboratory in Frascati (Rome) is a Xmon qubit coupled to a $\lambda/4$ resonator for readout. A diagram of the system is present in Fig. 3.2.

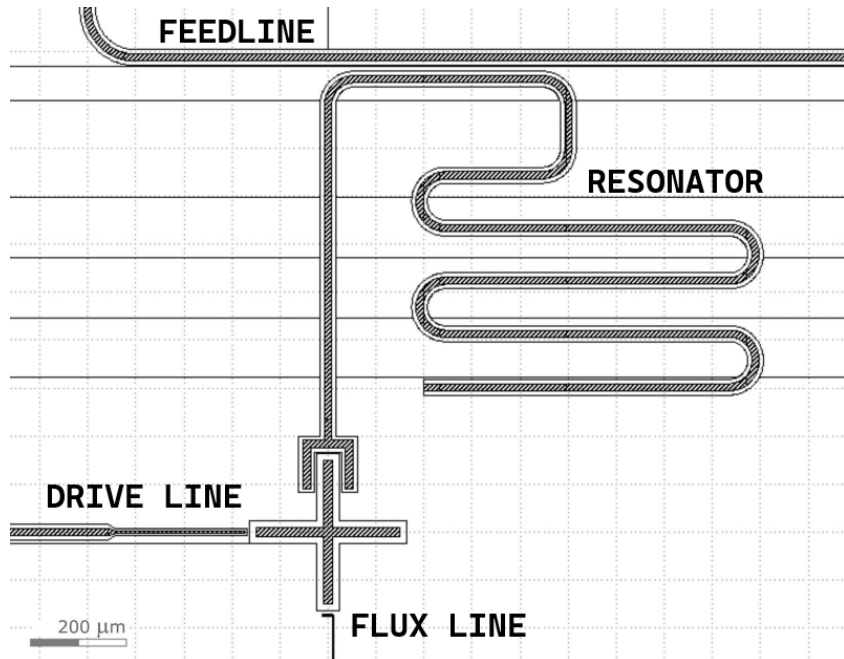


Figure 3.1: Design of the Xmon qubit coupled with the $\lambda/4$ resonator.[7]

The Xmon qubit is a type of transmon qubit and it is widely used in superconducting quantum computing. The Xmon qubit is currently the state-of-the-art qubit for many reasons. For starters the coherence time of the Xmon exceeds the one of a classical transmon qubit. This is done by grounding the transmon circuit reducing the electric field density and reducing the effect of the charge noise. They are known for their high fidelity, i.e. low error rate, even when coupled with other qubits.

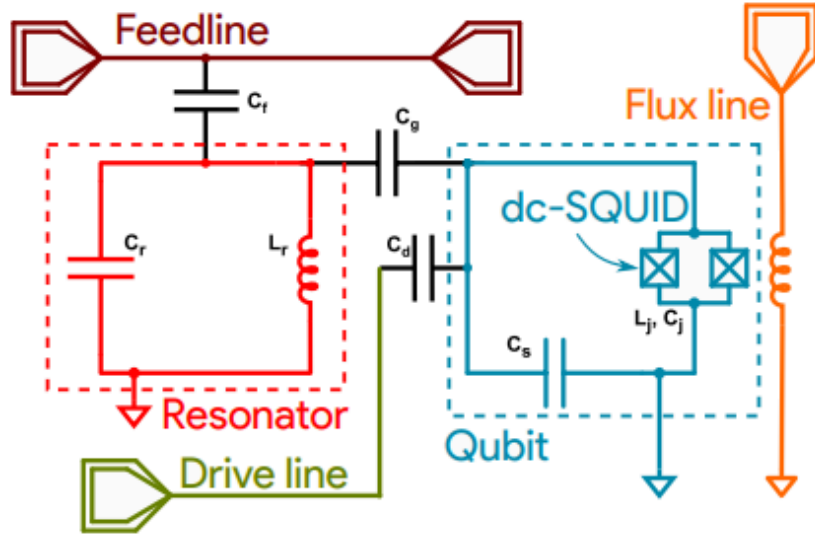


Figure 3.2: Diagram of the Xmon circuit. It can be observed that the transmon circuit and the resonator are both grounded. This is done to reduce the noise and, therefore, lower the error rate of the qubit.

The cross shape of the qubit allows for an easy connectivity. The four arms each posses a different role:

The arm on the top of the qubit in Fig. 3.1, is coupled to a coplanar waveguide (CPW) resonator, which is necessary for readout. We use the resonator as a substitute for the cavity. The main advantages of the resonator is its compact size, as it is much smaller than three dimensional cavity and it allows easier applications of multi qubit processors and a better coupling and precision. [4]

As seen in Fig. 3.2, the resonator is equivalent to a RLC parallel circuit. Considering a transmission line with characteristic impedance Z_0 of length $l = \lambda/4$, where λ is the wavelength of the resonance frequency, short circuited on one side ($x = 0$) and open on the other side ($x = -l$), and the propagation constant $\gamma = \alpha + j\beta$ we can identify the equivalent resistance, capacitor and inductance.

$$R = \frac{Z_0}{\alpha l}, \quad C = \frac{\pi}{4\omega_0 Z_0}, \quad L = \frac{1}{\omega_0^2 C}$$

The unloaded quality factor Q is :

$$Q = \omega_0 RC = \frac{\pi}{4\alpha l} = \frac{\beta}{2\alpha}$$

where $l = \pi/2\beta$ at resonance [5]. Considering a resonator at 6GHz frequency, character-

istic impedance of 50Ω and effective dielectric constant $\epsilon_{eff} = 5.2$, we get:

$$l = \frac{2\pi c}{4\sqrt{\epsilon_{eff}\omega_0}} = 5.5mm$$

$$Q_0 = 714,000$$

The arm on the right of the Xmon qubit is linked to the quantum bus, this is not present in Fig. 3.1 as not implemented in the Qub-IT project. The quantum bus is used to link two or more qubit in order to create coupled qubits, as depicted in Fig. 3.3. In Fig. 3.4 it's possible to see five coupled qubit connected through the quantum bus. In this picture is noticeable the easy scalability of the Xmon qubit.

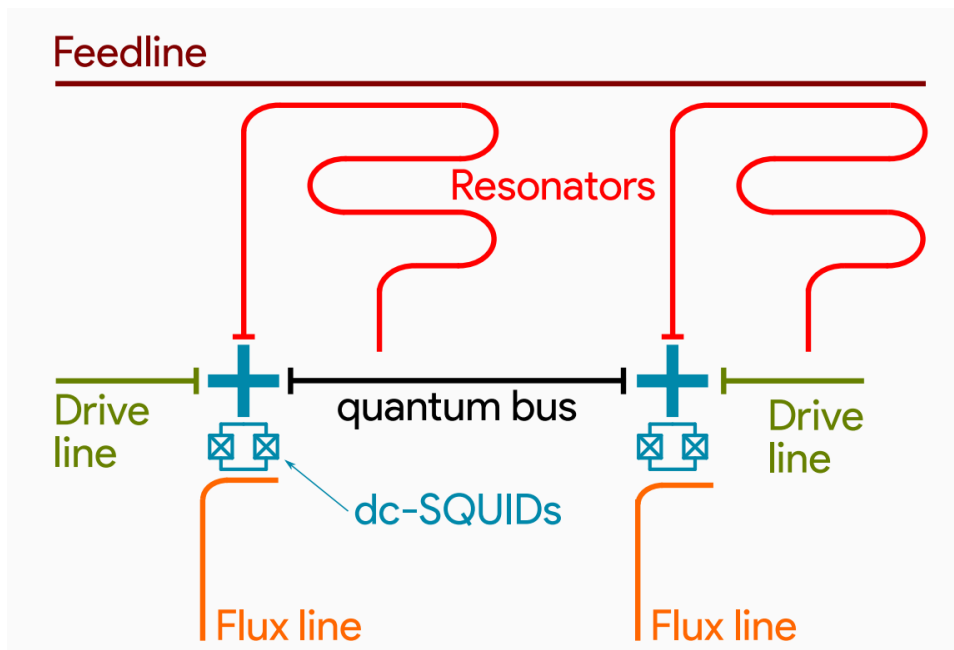


Figure 3.3: Two Xmon qubit connected via quantum bus

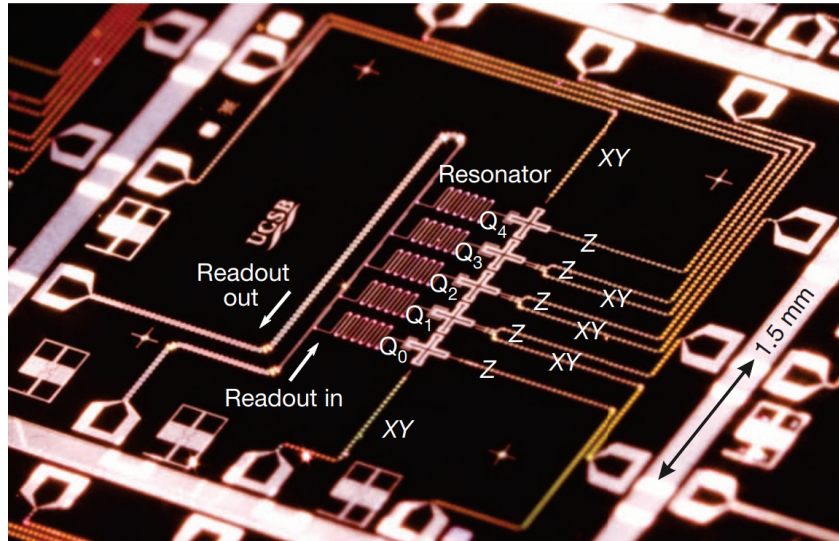


Figure 3.4: Optical image of a five coupled Xmon qubit placed in a linear array. The coupling uses direct connection between qubits.[2]

The other two are used to control the qubit: the drive line, shown in the left arm of the Xmon qubit in Fig. 3.1 allows to apply the X and Y quantum gates to the qubit (that represent a rotation around the X or Y axis on the Bloch Sphere) using pulses of microwaves, to excite the qubit and enable fast qubit control; the other one is the flux line, present in the bottom arm in Fig. 3.1, changes the magnetic flux in the SQUID. It's used to apply a Z quantum gate to the system, to achieve frequency control and so the tuning of qubit's energy spacing between the excitation levels.

In Fig. 3.5 is shown a representation of the chip used in the Frascati National Laboratory (FNL). This chip contains two qubit: one is a fixed-frequency resonator driven transmon, containing a Josephson Junction, and the other is a tunable-frequency transmon with dedicated drive-line, containing a DC-SQUID.

We use aluminium as superconductor on top of a $600\mu\text{m}$ silicon substrate, while the metal part is made of Niobium. [6]

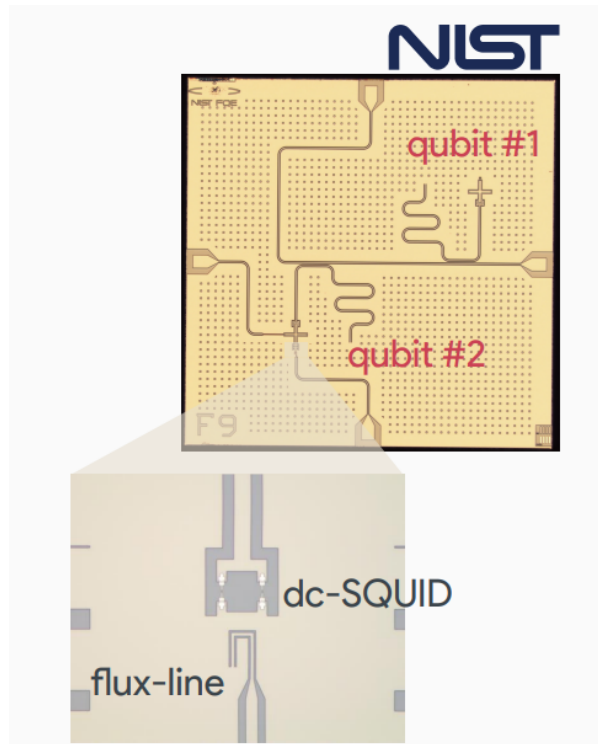


Figure 3.5: Representation of the chip containing two qubits. Qubit#1 is a fixed-frequency resonator driven transmon, while qubit #2 is a tunable-frequency transmon with dedicated drive-line. In fact it is possible to see in the second qubit the drive line and the flux line, lacking in the first qubit.

In the qubit design the Xmon cross has dimensions $21 \mu m$ width and $342 \mu m$ length, with $14 \mu m$ of a gap from the ground plane. The CPW readout resonator measures 4.689 mm in length, with trace width of $15 \mu m$ and a $9 \mu m$ gap, and a characteristic impedance of $Z_0 = 50\Omega$. The resonator is capacitively coupled to the feedline through a $500\mu m$ coupling trait $30\mu m$ distant from the feedline [7]. Knowing the dimension of the resonator we can find the cavity resonance frequency:

$$f_c = \frac{\omega_c}{2\pi} \sim 7.4395 \text{ GHz}$$

The team in Frascati is actually solving a problem in the assembly process that has impacted on the quality of the data taken in May. One of the Op-Amp inside the refrigerator wasn't correctly welded, so it didn't manage to amplify the signals correctly. The team is planning to reassembling the qubit correctly and to collect another set of data this December, that will provide more reliable result and will replace the ones taken in may.

3.2 Qubit characterization

After the construction of the qubit chip, it is necessary to measure its characteristics. Due to the size of the qubit and the low voltage sensibility used, the system needs to be cooled down. The energy of the temperature needs to be much smaller than the energy contained in the qubit, so $T \ll \frac{\hbar\omega_q}{k}$. This means the temperature of the qubit, at the moment of the measurement, have to be around 10mK. To do this the qubit is placed inside a dilution refrigerator that is able to keep the system at the low temperature we need. Pictures of the dilution refrigerator are shown in Fig. 3.6.

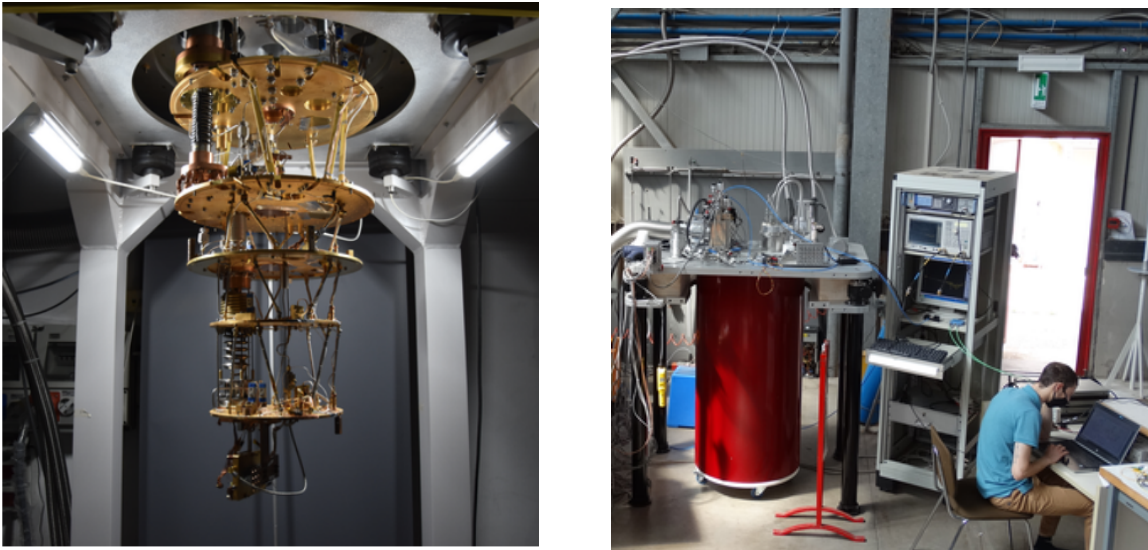


Figure 3.6: Pictures of the dilution refrigerator in the FNL in which the qubit is kept when measuring.[11]

To perform a basic qubit characterization it's necessary to perform five measurements:

- One-tone spectroscopy
- Two-tone spectroscopy
- Rabi Measurement
- T_1 Measurement
- T_2^* Measurement

It hasn't been possible to perform the T_2^* measurement, since the T_1 resulted too low to be able to perform a Ramsey measurement as described below.

Between the 6th and the 15th of May the team performed the first four experiment at Frascati National Laboratory. In the following sections I will present the results obtained analyzing these data.

3.2.1 Input Output Theory

Vector Network Analyzer

To perform the measurement of the qubit we use a Vector Network Analyzer (VNA). The VNA is a test instrument used in a wide range of radiofrequency (RF) and higher frequency applications. VNAs are used to validate the performance of many devices.

The VNA contains both a signal generator and a set of receivers. A signal is being sent to the device under test (DUT), then it measures both the input signal and output signal. Any difference between the two signals shows the effect of the DUT on the signal that passed through it (Fig. 3.7).

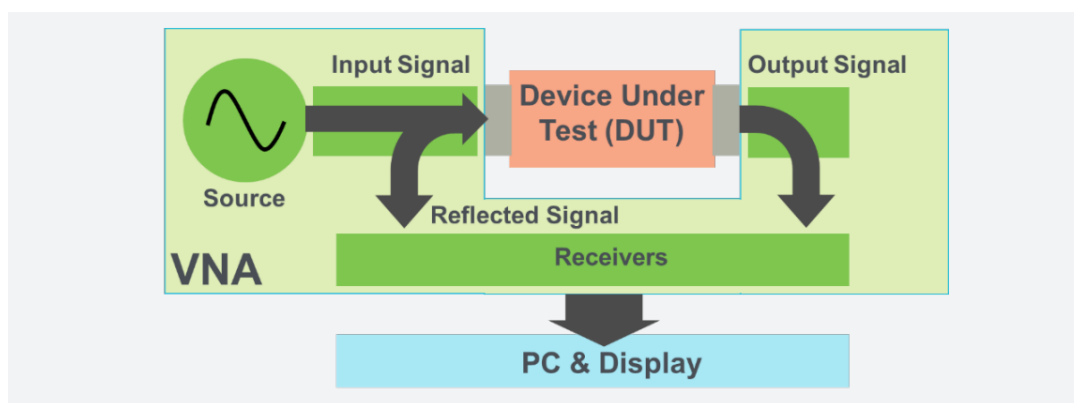


Figure 3.7: Schematic of how the VNA works

When working with high frequency signals it is difficult to measure current or voltage. It is common to measure the scatter parameters, or S-parameters. To understand the S-parameters, it's necessary to understand how a VNA works. Considering a 2-port VNA, they are typically both connected to the DUT, one for input and the other for output. The waves entering the DUT are called incident waves, part of this waves is transmitted as the output of the DUT and some is reflected back to the source. We can assign to each of the wave a phasor, the incident signal is a_n and the reflected or transmitted signal is b_n , where n correspond to the port number. For example, if the incident wave enters through the port 1 and the output goes through the port 2, we have that a_1 represents the incident signal, b_1 the reflected signal and b_2 the transmitted signal. Every one of these signals is measured by the VNA.

The S-parameters are defined as the ratios of signals coming from different ports. Using the signals from the previous example, we have:

$$S_{11} = \frac{b_1}{a_1} = \frac{\text{Reflected}}{\text{Incident}} \quad (3.1)$$

$$S_{21} = \frac{b_2}{a_1} = \frac{\text{Transmitted}}{\text{Incident}} \quad (3.2)$$

For the qubit characterization we are most interested in the S_{21} parameter.[9]

IQ Mixer

To perform the experiments we need to accurately be able to send signals with proper timing and duration. To do this we use RF IQ mixers, used for modulation and demodulation. A local oscillator (LO) is used to produce a signal, which is then divided in two identical quadrature signals, i.e. signals with 90° phase difference. So we get the LO with oscillations ω_L , that is divided in sine and cosine, which are two quadrature signals. By convention it's assigned I (In-phase) as the amplitude of the "in phase" signal and Q (Quadrature) as the amplitude of the 90° shifted signal. We can change I and Q independently, so the signal in I and the signal in Q doesn't have to be the same signal in quadrature but it can be changed accordingly to what we need. So we get $I(t) \cdot \cos(\omega_L t)$ and $Q(t) \cdot \sin(\omega_L t)$. The I and Q signals are then mixed to produce an output. By changing I and Q it's possible to modulate the amplitude, phase and frequency. A representation of the IQ mixer is shown in Fig. 3.8. The RF output is given by the addition of the two:

$$\text{Output} = I(t)\cos(\omega_L t) + Q(t)\sin(\omega_L t) \quad (3.3)$$

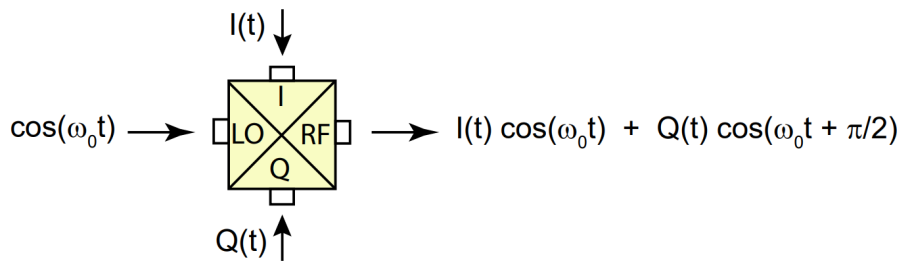


Figure 3.8: IQ Mixer

Here is given an example of phase modulation: if $I = Q$, it's produced an output with 45° phase with respect to the in phase signal. If $I = 0$ and $Q = 1$, the output has 90° phase, and if $I = 1$ and $Q = 0$ it has 0° phase.

A common way to represent IQ mixer is to use the phasor diagram, shown in Fig. 3.9.

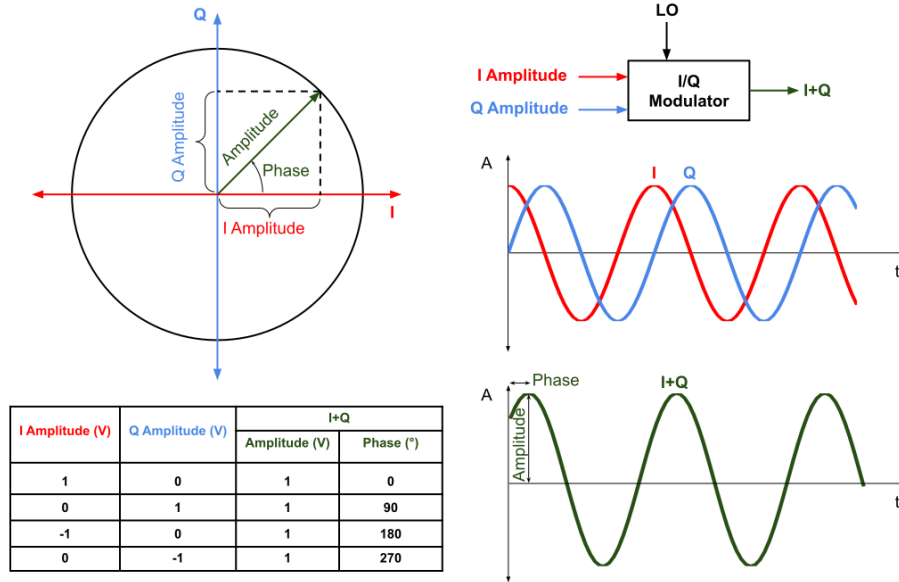


Figure 3.9: Phasor diagram of a IQ mixer

The amplitude ρ and the phase ϕ of the output wave can be calculated as:

$$\rho = \sqrt{I^2 + Q^2} \quad (3.4)$$

$$\phi = \tan^{-1} \frac{I}{Q} \quad (3.5)$$

In our scope, we use the IQ mixer also as a switch. By using a squared pulse on port I or Q, we can send the LO signal continuously and switch it on or off when needed. The RF output will always be zero, and it will transmit the LO signal only when the squared pulse is sent on port I or Q. This is represented graphically in Fig. 3.10.

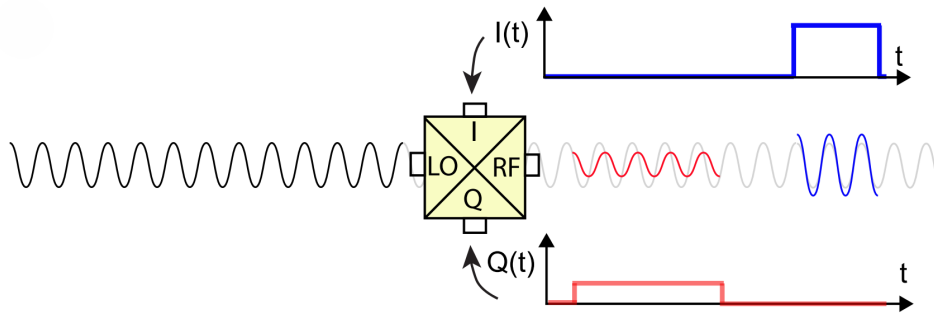


Figure 3.10: The LO signal is sent continuously, when a squared pulse is applied on I or Q, the signal is sent as RF output

For example, when it's used on the drive port of the qubit, by applying squared pulses on I or Q, it is possible to change the state of the qubit. By choosing the duration of the pulse, we can prepare the qubit in the excited state. The pulse on I correspond to a rotation around the X axis on the Bloch sphere, and on Q correspond to a rotation around the Y axis (Fig. 3.11).

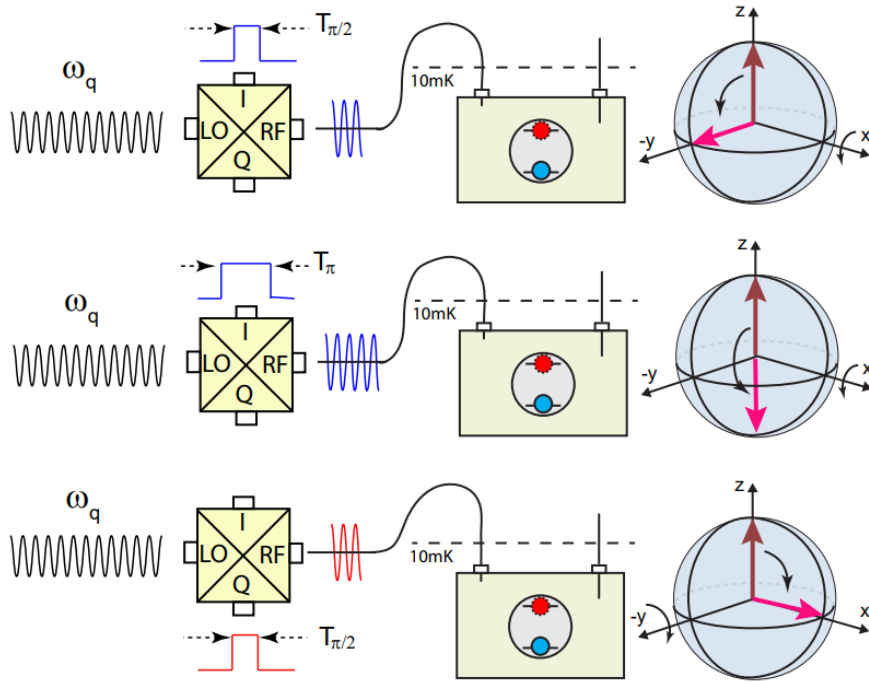


Figure 3.11: Applying a squared pulse on I of duration $\pi/2$ represent a rotation on the qubit around the X axis by 90° . Longer the duration of the pulse, bigger the rotation on the Bloch sphere. For a pulse of duration π , we have a half rotation. The system from the ground state is brought to the excited state. The same can be said when the pulse is applied on Q, but instead of the X axis, the rotation happens around the Y axis.

Readout

After manipulating the qubit state, we have to measure it. This is done by sending a signal with frequency ω_c to the $\lambda/4$ resonator. Once the signal is sent, using the VNA it's possible to measure both the signal sent to the resonator and the one transmitted back from it. Then the transmitted signal is demodulated with the incident one. The resulting IQ signal from the demodulation corresponds to the phase difference between the two. Basically we get to see how the signal has been changed when passing through the qubit. By reading this signal we can conclude if the resonant frequency of the system have been shifted up or down, and so if the system is in a bare, dressed or polariton state. The schematics of the readout is shown in Fig. 3.12.

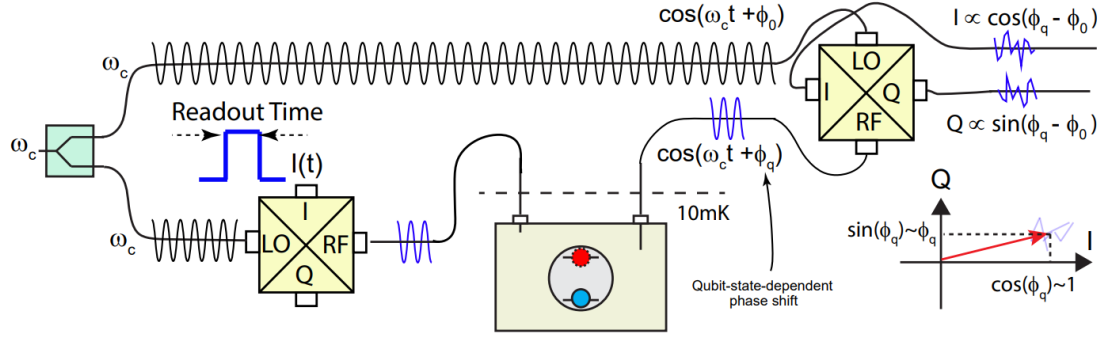


Figure 3.12: The signal is sent to the qubit through an IQ mixer, then it is demodulated when exiting the qubit with the same signal taken before entering the qubit. ϕ_0 represent the phase of the first signal due to the different path taken to the first, ϕ_q represent the difference in phase acquired by passing through the qubit.

3.2.2 One-Tone Spectroscopy

The first measurement we need to make on the qubit is the one-tone spectroscopy, or "Punch-Out". Basically we send the cavity a signal at different powers. We don't need to know the qubit frequency to perform this experiment. This experiment is done to check if the qubit interacts correctly with the cavity.

When we send signals at low power we know that the qubit is in the ground state. The Hamiltonian of this state is given by Eq. 2.49, where we get that the cavity frequency is shifted from its bare state by $-\chi$.

When we increase the power of the signal, the cavity frequency undergo a shift. This happens because sending a signal with high enough power it's like sending a huge amount of photons into the cavity, which overwhelm the qubit. In this situation the induced current on the qubit exceeds the critical current and the JJ lose its non-linearity. In this state it's as if there is no interaction between the qubit and the cavity, so the cavity frequency is the one from its bare state.

To conclude, if there is a shift in the cavity frequency from low to high power, this means that there is an interaction between the qubit and the cavity.

Furthermore, since $\chi = g^2/\Delta$, if we see that the bare frequency shift toward a lower frequency we will know that $\Delta > 0$, while if the shift is toward an higher frequency $\Delta < 0$, where $\Delta = \omega_q - \omega_c$ is the detuning. After having measured the qubit frequency in the next section, it's possible to roughly estimate the shift to estimate the coupling strength g . The bigger the shift in frequency, the bigger the coupling strength.

The data I analysed included a series of frequency sweeps at different power levels, from 0 dBm to -40 dBm, where dBm stands for decibel milliwatt, a unit measure of

power that is defined as:

$$P(x \text{ in mW}) = 10 \log \left(\frac{x}{1 \text{ mW}} \right) \quad (3.6)$$

For each sweep, the VNA is used to measure the S21 parameter of the signal. For frequencies near the resonance frequency, the S21 will be lower due to the fact that the energy of the signal will be absorbed by the cavity if it has the same frequency. For other frequencies the signal will not change significantly.

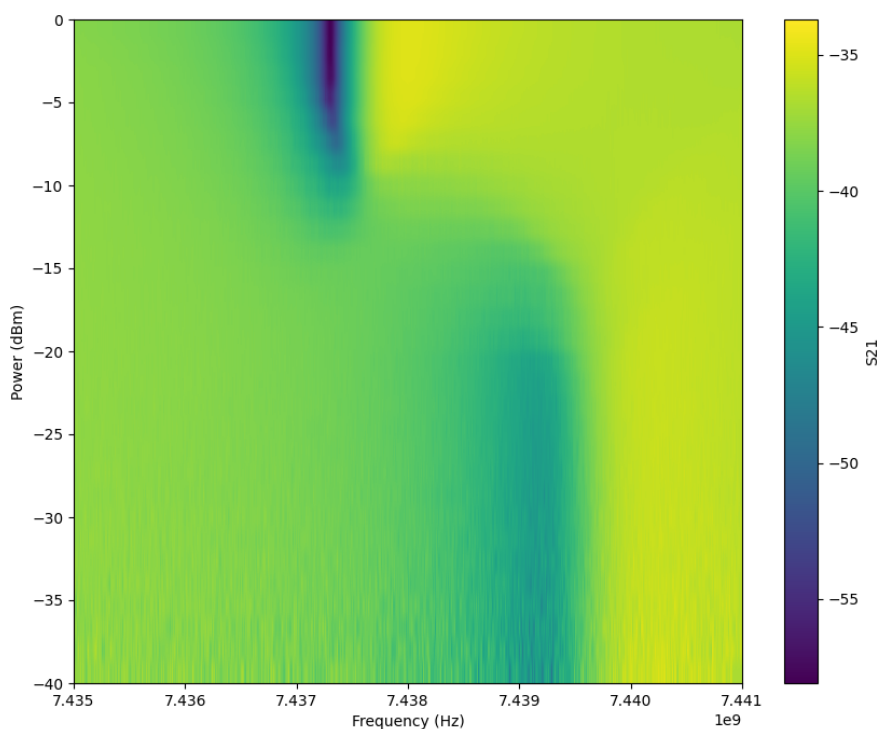


Figure 3.13: One-Tone spectroscopy of the qubit. This image represent the S21 in function of the cavity frequency and the power of the signal. Darker colors correspond to a lower S21, i.e. the transmitted wave has lower amplitude than the incident one. In this point the incident signal was in resonance with the cavity and lost energy. It's evident the shift of the cavity frequency between the -15dBm and -10dBm, and so we get at what power level the state of the qubit begins to change.

In Fig. 3.13 it is possible to see how the cavity frequency changes with the power. When the power is low, the cavity frequency in the dressed state is between 7.439 and

7.440 GHz. As the power increase, near the -15dBm or -10dBm mark, we get a direct shift of the cavity frequency. The bare cavity frequency is between 7.437 and 7.438 GHz. So we get a shift of ~ 2 MHz. From this we get that the dispersive shift χ is equal to:

$$\chi = \omega_c - \omega'_c = 2\pi(f_c - f'_c) \approx 2\pi(-2\text{MHz}) = -12.56\text{MHz} \quad (3.7)$$

Since χ is negative, we get that the Δ is also negative and the qubit frequency will be lower than the cavity frequency. The qubit is showing signs of working correctly.

3.2.3 Two-Tone Spectroscopy

We now want to measure the qubit frequency. To do this we send two signals, one to the drive and one to the readout. We keep the power low with the drive signal, so that the qubit remains in the ground state except when the frequency of the signal will be the qubit frequency. With a low power the probability that the qubit will be found excited in a frequency different from the qubit frequency become lower. Then we do various sweeps of the readout frequencies, each with a different frequency of the drive signal. We expect that the readout resonant frequency will be constant, as we can see in Fig. 3.14, until the drive signal excite the qubit. At this point the energy of the system changes, since the state of the qubit change from $|g\rangle$ to $|e\rangle$, and the cavity frequency shifts to a lower frequency.

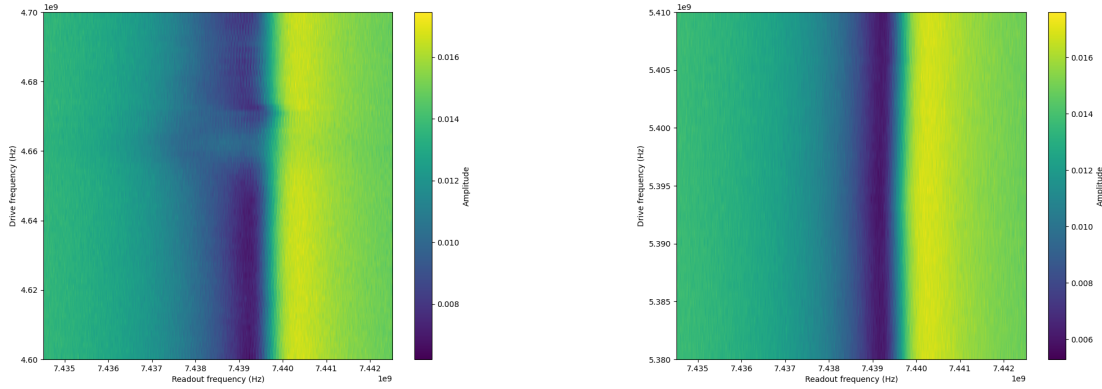


Figure 3.14: Two-Tone spectroscopy of the qubit. This image represent the amplitude of the transmitted signal in function of the cavity frequency and the drive frequency. These are attempts at finding the qubit frequency. In this graphs the cavity frequency is constant, meaning we are far from the qubit frequency.

Once the drive signal reaches the qubit frequency ω_q , the qubit is excited. When the cavity frequency changes we will know the qubit frequency. The measurement are

possible using IQ demodulation. We can find the amplitude of the wave by using Eq. 3.4.

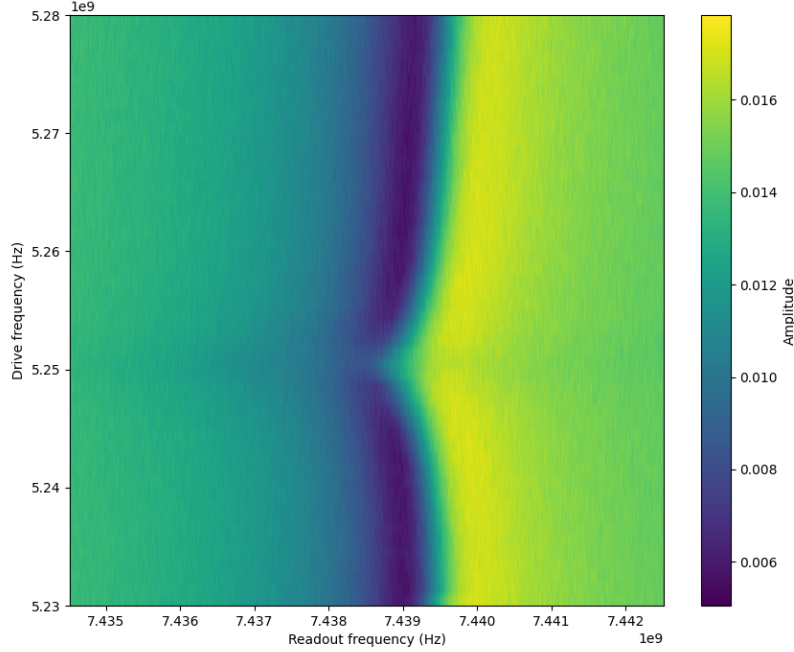


Figure 3.15: Two-Tone spectroscopy of the qubit. This image represent the amplitude of the transmitted signal in function of the cavity frequency and the drive frequency. Darker colors correspond to a lower amplitude, and indicates the resonance frequency of the qubit system. In this graph we can see the point where the state of the qubit changes, which tell us the frequency of the qubit.

In Fig. 3.15 we can see the points where the amplitude is lower. These zones correspond to the cavity resonance frequency. This frequency is constant until we reach the qubit frequency, which in this case is about 5.25GHz. This value is within our expectations, since from the One-Tone Spectroscopy we saw that $\omega_q < \omega_c$. We can calculate the detuning of the qubit-cavity system:

$$\Delta = \omega_q - \omega_c \approx (5.25 - 7.44)\text{GHz} = -2.19\text{GHz} \quad (3.8)$$

From this we can get a rough estimation of the parameter g:

$$g = \sqrt{\chi \cdot \Delta} \approx \sqrt{(-12.56\text{MHz}) \cdot (-2.19 \cdot 10^3\text{MHz})} = 166\text{MHz} \quad (3.9)$$

3.2.4 Rabi Measurements

We now know the qubit frequency and we want to study what happens to the time evolution of the qubit when we send a signal to the drive line. We want to see the Rabi oscillation, which are the oscillation of the qubit state over time.

We can send a drive signal at qubit frequency ω_q using the IQ mixer as a switch. As mentioned below, by sending a squared signal, either by the I port or the Q port, we can select a length of time that indicates the duration of the drive signal. By doing this we can control how long the signal will last with great accuracy. To perform the experiment we need to send the drive signal that will last a time t and, right after that, send a readout signal to scope the state of the qubit. This experiment is repeated for different time duration t of the drive signal, and for each t the experiment is repeated N times to get a small error.

In Fig. 3.16 is represented a schematic of the circuitry of the experiment. The BNC1 represent the readout signal that has frequency equal to the cavity resonance frequency, while BNC2 represent the drive signal that has frequency equal to the frequency qubit. Both signal is continuous and is modulated using the IQ mixers. In fact AWG Ch1 is a squared signal that correspond the I signal and controls the drive signal, while AWG Ch2 is also a squared signal that corresponds to the Q signal that controls the Readout signal. We can see how the drive signal has a duration of time t while the readout is off, and as soon as the drive is shut down, the readout is turned on. The input is a composition of the two signal, while the output correspond to the transmitted readout signal. This transmitted readout signal is then demodulated with the incident readout signal using an IQ mixer, that gives an I and Q signal that is then collected. By using Eq. 3.4 it's possible to measure the amplitude of the output signal.

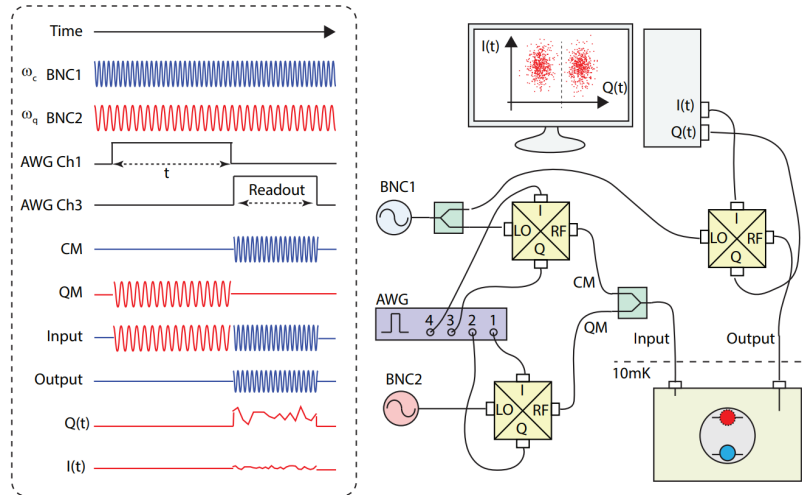


Figure 3.16: Circuitry of the Rabi measurements

For each time duration of the drive signal the experiment has been repeated for about 100 times. To accurately measure the Rabi oscillations, I have taken the average of these 100 measurement and plotted the result. Starting with a low time duration t in Fig. 3.17, with $t = 5 \cdot 10^{-8}$ s, we can see both a readout which have the drive before it and a readout without the drive to compare the effect of the drive on the oscillations. In red we represent the drive signal, in green the readout signal and in blue the amplitude of the output signal.

It is possible to see in Fig. 3.17 a lowering in the amplitude right after the readout signals have been switched on, in both the readout signals. Probably this is caused by a reflexive effect, before the wave becomes stationary. Only after the wave has found stationarity, it becomes harmonic. Before this happens, the wave is not harmonic and a component is reflected so transmission is lower, and that is probably why we see the lowering of the S21-parameter stated before.

In Fig. 3.17 there is not much difference between the lowering on the first readout and the lowering on the second one, probably because the drive time is too low to have any impact on the state of the qubit.

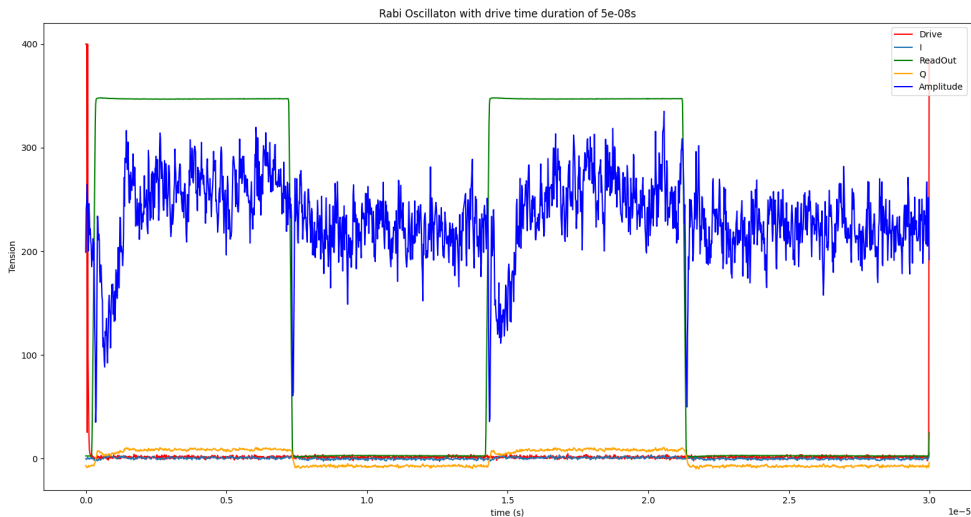


Figure 3.17: Rabi oscillation with the time duration of the drive signal of $t = 5 \cdot 10^{-8}$ s. To the left the readout right after the drive, to the right a readout signal without excitation for comparison. This data has been averaged between 106 repetition of the experiment. The amplitude tension has been magnified by 30 times for better clarity. We can see how the side with the drive has no apparent difference with the one without the drive.

The highest time duration of the drive signal measured in the FNL correspond to the one in Fig. 3.18, where we have a duration time of $t = 1 \cdot 10^{-6}$ s. In this plot the lowering

caused by the readout is still present but it's different between the readout with the drive and the one without it. We can see how, at the start of the readout the lowering is less pronounced, probably because the longer drive gives more energy to the qubit, causing an increase of the amplitude of the Rabi oscillations.

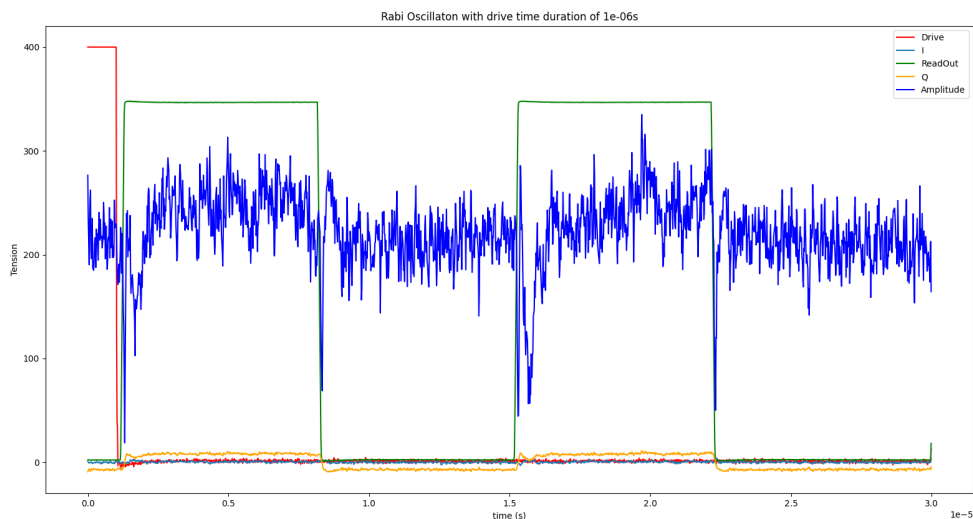


Figure 3.18: Rabi oscillation with the time duration of the drive signal of $t = 1 \cdot 10^{-6}$ s. To the left the readout right after the drive, to the right a readout signal without excitation for comparison. This data has been averaged between 106 repetition of the experiment. The amplitude tension has been magnified by 30 times for better clarity. The left graph shows an higher amplitude than the one on the left.

In Fig. 3.19 we see a comparison between the two signals. The signal with the lowest drive time has a bigger leap than the the one with a high drive time.

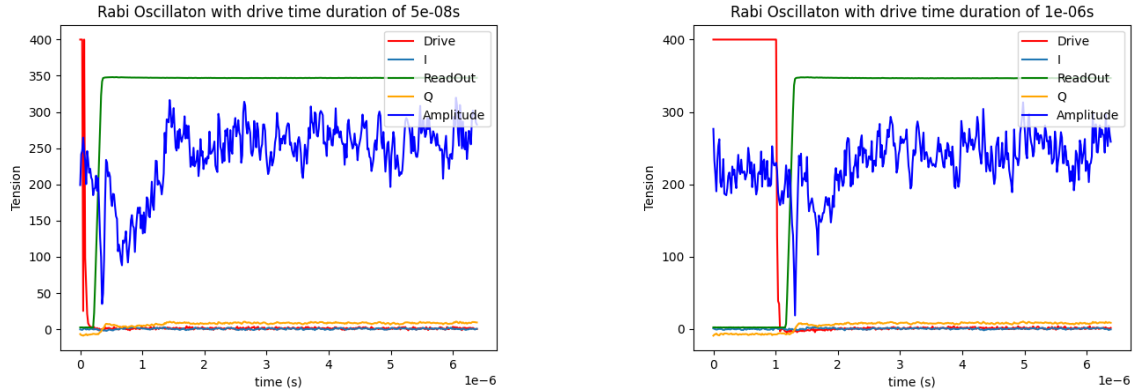


Figure 3.19: To the left the Rabi oscillations with drive time $t = 5 \cdot 10^{-8}$ s, to the right the Rabi oscillations with $t = 1 \cdot 10^{-6}$ s. We can see how the lowering of the amplitude in the first case is bigger then the second.

The lowering of the amplitude at the start of the readout actually prevents us to actually see the correct Rabi oscillations. To get around this problem the team at Frascati thought of taking the data in another way. To evade the problem of the amplitude getting lower at the started of the readout, they decided to switch on the drive signal while the readout was also on. In this way the oscillations where more clear. To see a Rabi oscillation without the lowering at the start of the readout, we can first apply the readout and, after that, the drive. In Fig. 3.20 we can see some screenshots of the oscillator present in the FNL. The oscillator automatically does an average of many periods of measurement. Each picture represent a different power level of the drive signal. The yellow line represent the readout, the red line represent the drive and the green line at the bottom represent the amplitude. When the amplitude is low it means that the readout is turned off, and that means that we can't read the state of the qubit. The moment it is switched on we can see the rise of the amplitude and also the same reflexive effect of above. When the drive is switched on we can see an oscillation in the amplitude, that is the Rabi oscillations we want to measure. At different power levels the oscillations are different. In the first image the drive has a power of -15dBm and the amplitude barely get above the ground level state. In the second image the drive signal has a power of -5dBm, we can see the amplitude getting higher then the one at ground level, but still no oscillation is present. At 5dBm, in the last image, we can clearly see the oscillations of the qubit as we expected to find them at the start. There is also a little delay between the drive signal and the start of the oscillation that shouldn't be there, probably caused by a delay in the equipment.

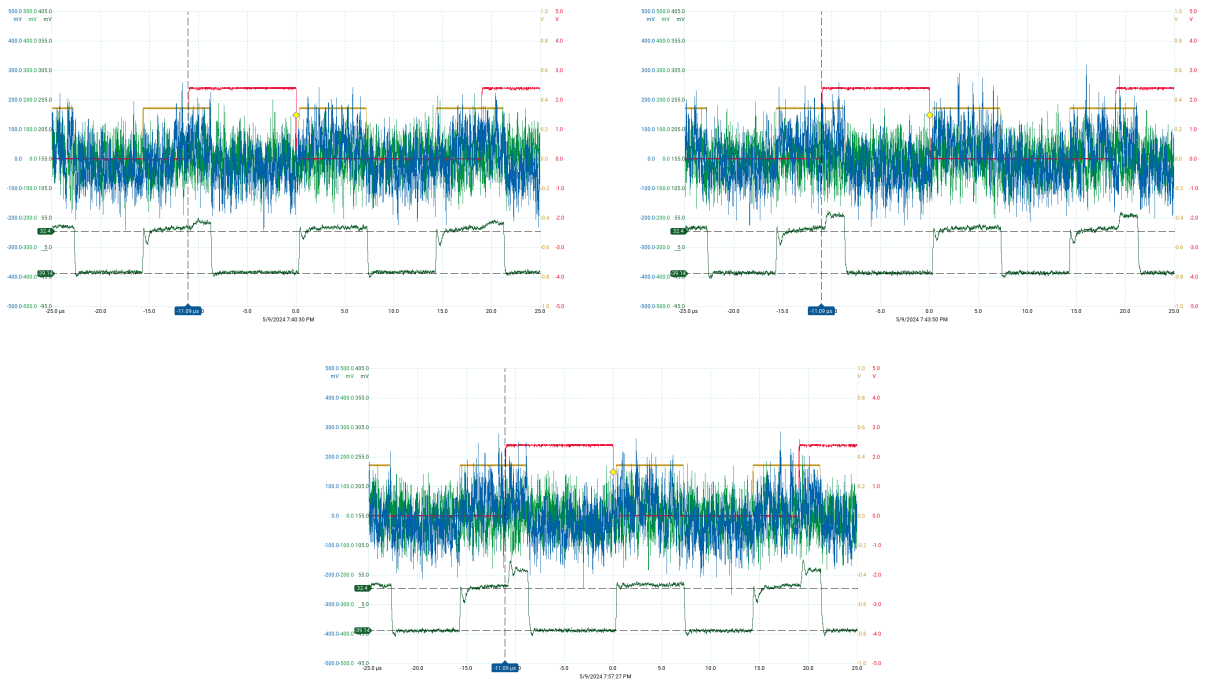


Figure 3.20: Rabi Oscillation at various power levels. The first at -15dBm , the second one at -5dBm and the last at 5dBm . The red line indicates the drive, the yellow line corresponds to the readout. The green line at the bottom corresponds to the amplitude of the transmitted wave. When the drive is on, it's possible to see the Rabi oscillations on the amplitude line.

We can also study the behaviour of the Rabi oscillations at different drive frequencies, near the qubit frequency. With this we can have a better estimation of the qubit frequency than with the Two-Tone Spectroscopy. By measuring the oscillations of the qubit at different drive frequencies, near the qubit frequency, it's possible to draw a 2D graph called the Chevron plot.

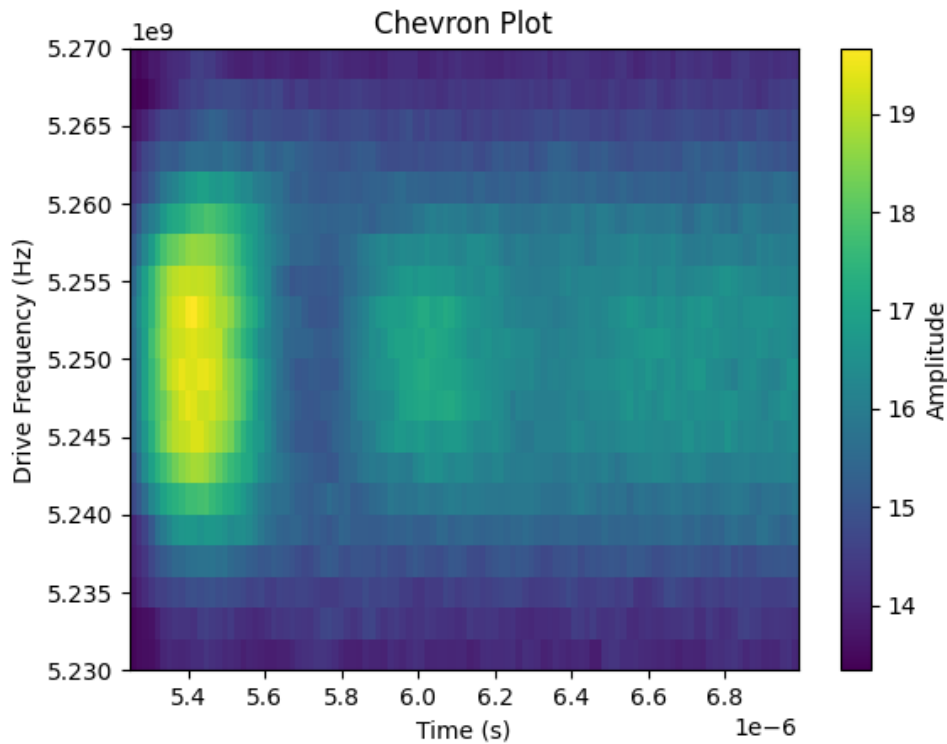


Figure 3.21: Chevron plot of the Qub-IT qubit, represent the amplitude of the wave in function of the time and the drive frequency.

By looking at Fig. 3.21 we can see how the amplitude of the oscillations decreases as we get away from the qubit frequency, at the center of the plot. This plot should also give us some information about the relaxation time of the qubit, as we can see for how long the qubit continues to oscillate between the ground and the excited state. In fact in Fig. 3.21 we see that the oscillations die almost immediately. We also expect that oscillations near the qubit frequency will have higher frequency, but as the relaxation time is so fast, it doesn't give us enough information to properly consider this aspect. Another view of the Rabi oscillations is in Fig. 3.23, where we can see some of the amplitudes at different frequencies in a one-dimension plot. From here we can see more clearly that the oscillations die very quickly and that, except for the amplitude with drive at qubit frequency, they can't manage to do even a single period.

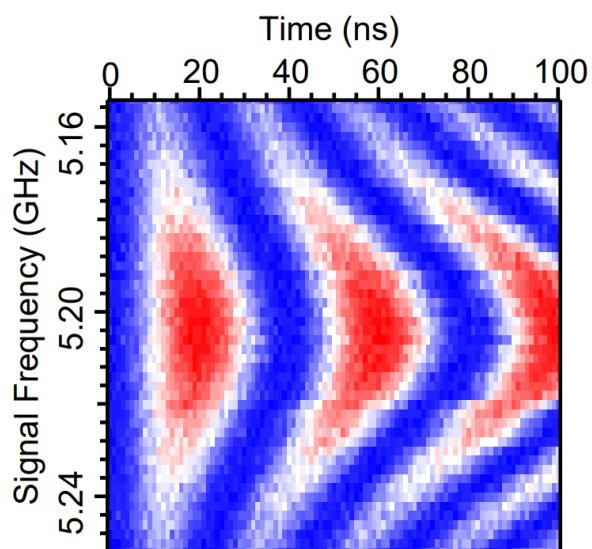


Figure 3.22: A typical result of the Chevron plot [3]

The expected Chevron plot should look like Fig. 3.22, where we can clearly see that the oscillations last much more time and the frequency of the Rabi oscillations at the border of the Chevron plot is higher, while at the center, corresponding to the frequency qubit, the amplitude is higher but the frequency is lower. We theorize that this problem is given by the assembly error mentioned above, as the incorrectly welded Op-Amp increased the temperature inside the refrigerator, it significantly disturbed the measurements of the qubit, that is very susceptible to external noise. This increase in temperature probably caused the qubit to relax faster his energy and so we got Rabi oscillations that die very quickly.

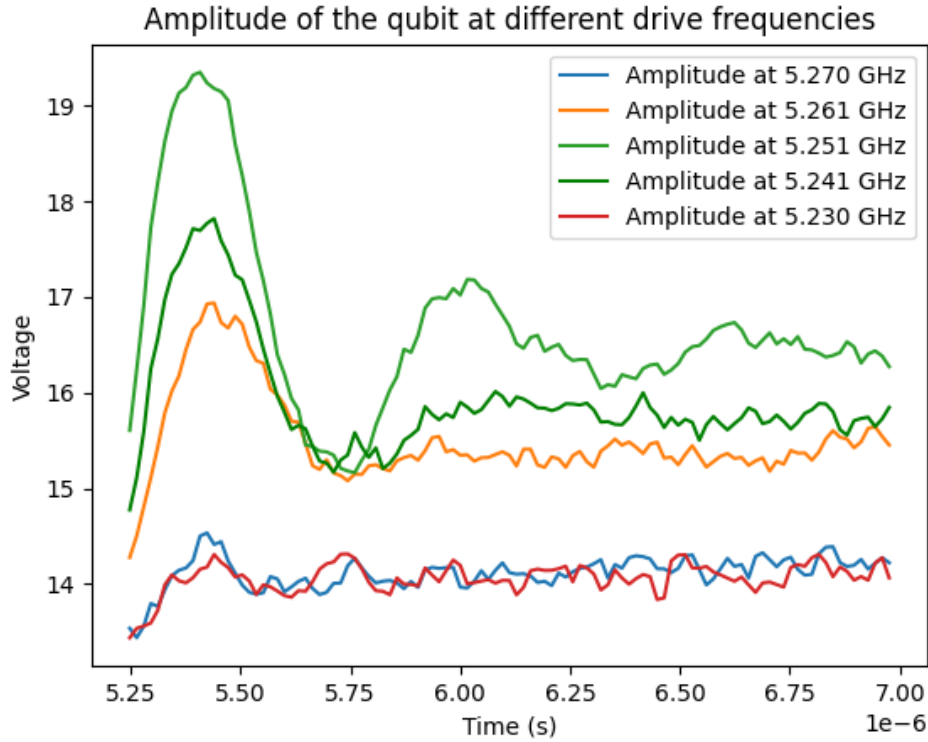


Figure 3.23: Rabi oscillations of the qubit at different drive frequencies. We can see how the biggest oscillations happens at qubit frequency, at $\sim 5.251\text{GHz}$, while other frequencies have lower amplitude and lower relaxation time.

3.2.5 T_1 Measurements

The T_1 represent the relaxation time of the qubit, i.e. the time in which the qubit can maintain the information of its state before collapsing, even without being measured. To measure T_1 we first prepare the qubit in the excited state. To do this we send a π -pulse drive signal to the qubit, that is a drive signal with exactly the time duration to make a 180° rotation of the x-axis, or the y-axis, in the Bloch sphere. By sending a π -pulse drive signal to the qubit we are effectively applying a Y gate (Fig. 3.24).

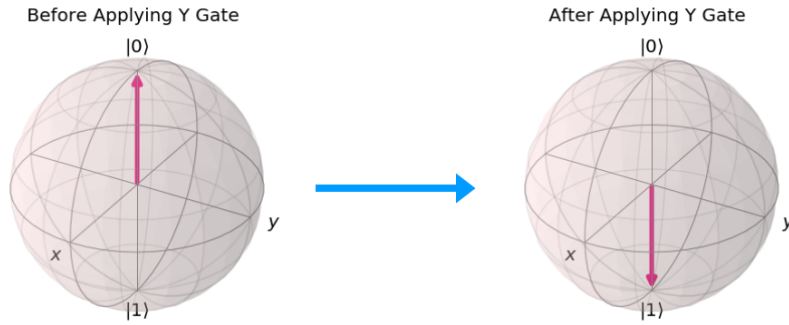


Figure 3.24: Representation of a Y gate on the Bloch sphere

After having prepared the qubit in the excited state, we want to know for how long it can remain in that state. So we wait for a time t and then switch on the readout, repeating the measurement for different delays between drive and readout. We continue to manipulate the input signals using IQ mixers and sending to I or Q squared wave functions, as shown in Fig. 3.25.

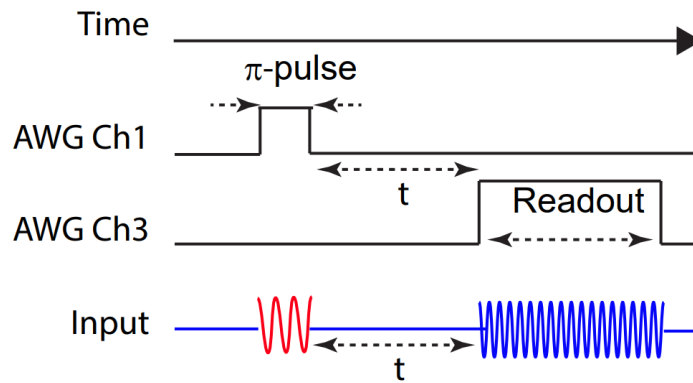


Figure 3.25: Diagram of the T_1 measurement

The data taken in the FNL on the T_1 measurement consist in 29 repetition of the experiment. Each repetition consisted in 12 measurement of the amplitude of the state of the qubit, at different delays between the π -pulse drive signal and the readout signal. I averaged these 29 data to get the lowest error possible and obtained 12 different amplitudes.

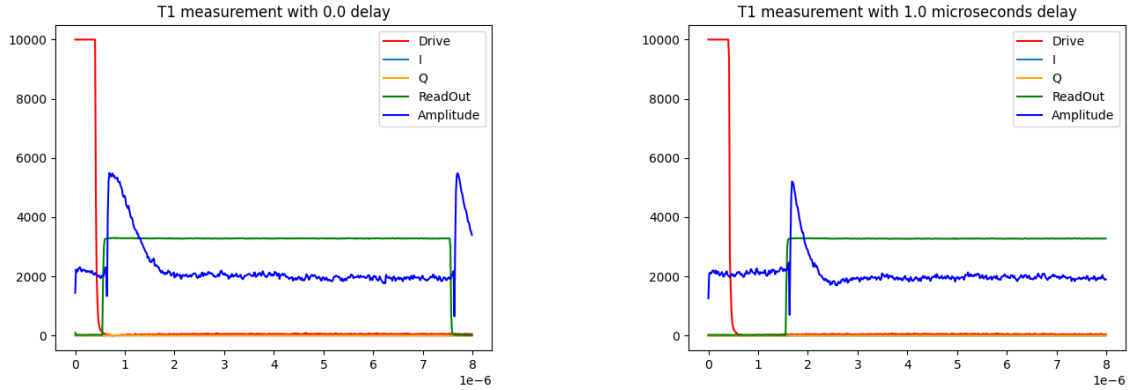


Figure 3.26: Graph representing the measurement of the qubit after different delays between the drive and the readout. It's possible to see how the qubit state with more delay decay faster than the one without delay. The amplitude line has been greatly zoomed to allow a clearer observation of the data.

In Fig.3.26 are represented 2 of the 12 amplitudes, the one with the lowest delay of 0s and the one with the biggest delay of $1\mu s$. Here we can see the behaviour of the different amplitudes. After the readout every amplitude spikes for an instant, and then rapidly decrease to a stable state. The T_1 is directly related to how fast the system return to the stable state.

We can consider that each amplitude has an exponential decay with different decay time, that it is apparently lower when the delay between readout and drive increases. We are interested in quantifying these time decays, to know how big they are and how they change in function of the delay, in order to measure the T_1 of the qubit. To do this I used the "scipy" library in Python in order to fit these amplitudes in an exponential fit of the type:

$$a \cdot e^{-t/\tau} + b \quad (3.10)$$

where a , τ and b are free parameters. By doing so I obtained the plots in Fig. 3.27, where we can see both the points that have been fitted and the fit in dashed line of the same amplitudes of above. These fits have a $\chi^2 \sim 0.99$, that means that the fit model represent with a high level of fidelity the original data. In these cases the decay time of these exponential fits, τ , is $5 \cdot 10^{-7}s$ for the amplitude with delay of 0s and $2.2 \cdot 10^{-7}s$ for the amplitude with delay of $1\mu s$, confirming quantitatively what we have seen in the previous graphs.

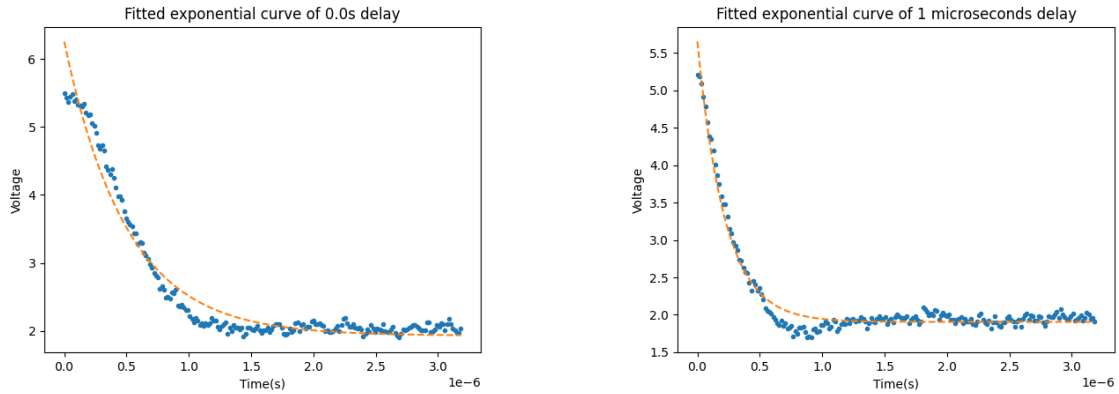


Figure 3.27: Exponential fit of the decay of the qubit ($e^{-\frac{t}{\tau}} + b$). On the left the decay with no delay with $\tau = 5 \cdot 10^{-7}$ s. On the right the decay of the qubit with delay of $1\mu\text{s}$ and $\tau = 2.2 \cdot 10^{-7}$ s

The fits has been repeated for each amplitude, obtaining 12 different decay times. By plotting these 12 decay times on a graph in function of the delays, we can see that it also assumes an exponential distribution. Then I fitted also this graph, using the same exponential function in Eq. 3.10. Doing so I plotted the graph in Fig. 3.28. This fit has an even better χ^2 of before, that is ~ 0.999 .

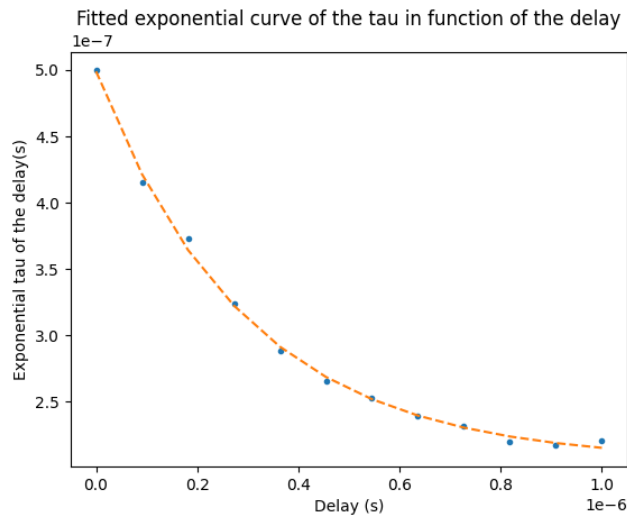


Figure 3.28: Exponential fit of the 12 decay times at different delays

The τ parameter of the fit in Fig. 3.28 will tell us the relaxation time of the qubit, that is $T_1 = 2.96 \cdot 10^{-7}$ s. This T_1 is much lower then expected, as already seen in the other

measurements. The estimated relaxation time for this qubit is $T_1 \sim 70\mu s$ [6], so of 2 order higher than what we got. As mentioned already, the probable cause for this error is the defective component that heated too much and made the temperature inside the refrigerator higher. As the environmental noise increased, the qubit started to relax its energy faster than expected.

Conclusions

The characterization of the superconductive qubit of the Qub-it project has provided an insight into its behaviour and parameters. Through the various measurements, like the One-tone spectroscopy and Two-tone spectroscopy, we managed to find the qubit's properties including the qubit frequency and the cavity frequency of the qubit. Using the Rabi oscillations we managed to see how accurately we can control the state of the qubit, and we calculated the T_1 relaxation time that measures for how long the qubit can maintain a given state before relaxing its energy. At last, the T_1 was too low to perform the Ramsey measurement and we couldn't determine the T_2^* of the qubit, i.e the decoherence time.

The lower-than-expected T_1 time was likely influenced by a problem discovered after the data was collected. One reason for that may be a problem that the team in Frascati found within the system, after the data was taken. Apparently one of the Op-Amp inside the qubit's refrigerator was welded incorrectly, so it didn't work properly and dissipated a lot of heat to the environment, causing some of the data to be of bad quality. Another set of data will be taken at the end of the year, after the mistake will be fixed. By doing this it's expected a longer time of relaxation of the qubit, as it will be more shielded from external noise.

This study will be important for the development of instruments with the ability to detect itinerant photons without absorbing them, the goal of the Qub-IT project. It represent a step towards the development of highly sensitive quantum sensors for the detection of axions, theorized particle and dark matter candidate.

The Qub-IT project is aimed at developing quantum sensing technologies using superconducting qubits for both current and future INFN experiments. The primary goal of the project is to create an itinerant single-photon counter that surpasses existing devices in terms of efficiency and minimizing dark-count rates. This is achieved through the use of repeated Quantum Non-Demolition (QND) measurements on a single photon.

In conclusion, this project successfully characterized the Qub-IT qubit, but additional measurements will be necessary for a more precise and complete characterization.

Bibliography

- [1] Michael A. Nielsen and Isaac L. Chuang. *Quantum Computation and Quantum Information, 10th Anniversary edition*. Cambridge University Press, New York, 2010. ISBN: 978-1-107-00217-3.
- [2] R.Barends and J.Kelly et al. “Superconducting quantum circuits at the surface code threshold for fault tolerance”. In: *Nature* (2014). DOI: 10.1038/nature13171.
- [3] Mahdi Naghiloo and Murch Lab. “Introduction to Experimental Quantum Measurement with Superconducting Qubits”. In: *arXiv* (2019). DOI: 10.48550/arXiv.1904.09291.
- [4] A. Mamgain and S.S.Khaire et al. “A Review of Developments in Superconducting Quantum Processors”. In: *Springer* (2022). DOI: 10.1007/s41745-022-00330-z.
- [5] Claudio Gatti. *Lectures on cQED*. 2023.
- [6] Andrea Giachero. *Development of transmon qubits for quantum sensing and computing*. 2024. URL: [https://nqsti-indico.fisica.unimib.it/event/18/contributions/46/attachments/40/66/giachero.NQSTI.2024%20-%20Andrea%20Giachero%20\(1\).pdf](https://nqsti-indico.fisica.unimib.it/event/18/contributions/46/attachments/40/66/giachero.NQSTI.2024%20-%20Andrea%20Giachero%20(1).pdf).
- [7] R.Moretti and H.A.Corti et al. “Design and simulation of a transmon qubit chip for Axion detection”. In: *IEEE* (2024). DOI: 10.1109/TASC.2024.3350582.
- [8] *Atom Computing Announces Record-Breaking 1,225-Qubit Quantum Computer*. URL: <https://moorinsightsstrategy.com/research-notes/atom-computing-announces-record-breaking-1225-qubit-quantum-computer/>.
- [9] *Introduction to VNA Basics*. URL: https://download.tek.com/document/70W_60918_0_Tek_VNA_PR.pdf.
- [10] Roberto Moretti. *QUANTUM SENSING WITH SUPERCONDUCTING QUBITS FOR FUNDAMENTAL PHYSICS*. URL: https://www.benasque.org/2023sqftalks_contr/2013_17_Abstract_Qub_IT_Roberto_Moretti.pdf.
- [11] *Qub-IT Pictures*. URL: <https://web.infn.it/qub-it/pictures/>.

